1

Motorcycle Dynamics

Vittore Cossalter, Roberto Lot, and Matteo Massaro
University of Padova, Italy

This chapter aims at giving a basic insight into the two-wheeled vehicle dynamics to be applied to vehicle modelling and control. The most relevant kinematic properties are discussed in Section 1.1, the peculiarities of motorcycle tyres are reported in Section 1.2, the most popular suspension schemes are presented in Section 1.3, while Sections 1.4 and 1.5 are devoted to the analysis of the vehicle in-plane and out-of-plane vibration modes. Finally, Section 1.6 highlights the coupling between in-plane and out-of-plane dynamics.

1.1 Kinematics

From the kinematic point of view, every mechanical system consists of a number of rigid bodies connected to each other by a number of joints. Each body has six degrees of freedom (DOF) since its position and orientation in the space are fully defined by six parameters, such as the three coordinates of a point (x, y, z) and three angles (yaw, roll, pitch). When a joint is included, the number of DOFs reduces according to the type of joint: the revolute joint (e.g., the one defining the motorcycle steering axis) inhibits five DOFs, the prismatic joint (e.g., the one defining the telescopic fork sliding axis) inhibits five DOFs, the wheel–road contact joint inhibits three DOFs when pure rolling is assumed (only three rotations about the contact point are allowed while no sliding is permitted), or one DOF when longitudinal and lateral slippage is allowed (the only constraint being in the vertical direction, where the compenetration between the wheel and the road is avoided).

1.1.1 Basics of Motorcycle Kinematics

Two-wheeled vehicles can be considered spatial mechanisms composed of six bodies:

- the rear wheel;
- the swingarm;

- the chassis (including saddle, tank, drivetrain, etc.);
- the handlebar (including rear view mirrors, headlamp, the upper part of the front suspension, etc.);
- the front usprung mass (i.e., the lower part of the front suspension, front brake calliper, etc.);
- the front wheel.

These bodies are connected each other and with the road surface by seven joints:

- a contact joint between the rear wheel and the road surface;
- a revolute joint between the rear wheel and the swingarm, to give the rear wheel spin axis;
- a revolute joint between the swingarm and the chassis, to give the swingarm pivot on the chassis;
- a revolute joint between the chassis and the handlebar, to give the steering axis;
- a prismatic joint between the handlebar and the front unsprung, to give the sliding axis of the telescopic fork;
- a revolute joint between the front unsprung and the front wheel, to give the front wheel spin axis;
- a contact joint between the front wheel and the road plane.

Therefore, the two-wheeled vehicle has nine DOFs, given the 20 DOFs inhibited by the four revolute joints, five DOFs inhibited by the prismatic joint and the two DOFs inhibited by the two contact joints (tyre slippage allowed), subtracted from the 36 DOFs related to the six rigid bodies. It is also common to include the rear and front tyre deformation due to the tyre compliance, and consequently the number of DOFs rises to 11.

Among the many different sets of 11 parameters that can be selected to define the vehicle configuration, it is common (e.g. Cossalter et al. 2011b, 2011c) to use the ones depicted in Figure 1.1: position and orientation of the chassis, steering angle, front suspension travel, swingarm rotation and wheel spin rotations.

Finally, it is worth mentioning that these DOFs are related to the gross motion of the vehicle, while additional DOFs are necessary whenever some kind of vehicle structural flexibility is considered, e.g. Cossalter et al. (2007b).
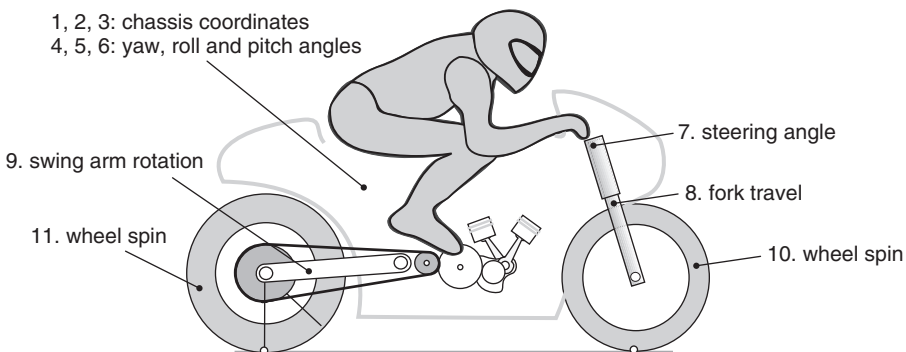

Figure 1.1   Degrees of freedom of a two-wheeled vehicle

Some geometric parameters such as the wheelbase p, normal trail a_n and caster angle ε, are very important when it comes to the vehicle stability, manoeuvrability and handling. In more detail, the wheelbase is the distance between the contact points on the road and usually ranges between 1.2 and 1.6 m, the normal trail is the distance between the front contact point and the steering axis (usually 80–120 mm) and the caster angle is the angle between the vertical axis and the steering axis (usually 19–35°).

In general, an increase in the wheelbase, assuming that the other parameters remain constant, leads to an unfavourable increase in the flexional and torsional deformability of the frame (this may reduce vehicle manoeuvrability), an unfavourable increase in the minimum curvature radius, a favourable decrease in the load transfer during accelerating and braking (this makes wheelie and stoppie more difficult) and a favourable increase in the directional stability of the motorcycle.

The trail and the caster angle are especially important inasmuch as they define the geometric characteristics of the steering head. The definition of the properties of manoeuvrability and directional stability of two-wheeled vehicles depend on these two parameters, among others. Small values of trail and caster characterize sport vehicles, while higher values are typical of touring and cruiser vehicles. The trail and caster are related to each other by the following relationship:

$$a_n = R_f \sin \varepsilon - d, \tag{1.1}$$

where R_f is the front tyre radius and d is the fork offset; see Figure 1.2.

Finally, it is worth noting that all these parameters are usually given for the nominal (standstill) trim configuration, while they change as the vehicle speed, longitudinal and lateral accelerations change.

1.1.2 Handlebar Steering Angle and Kinematic Steering Angle

While the driver operates the handlebar steering angle, the vehicle cornering behaviour is determined by the projection on the road surface of the angle between the rear and front
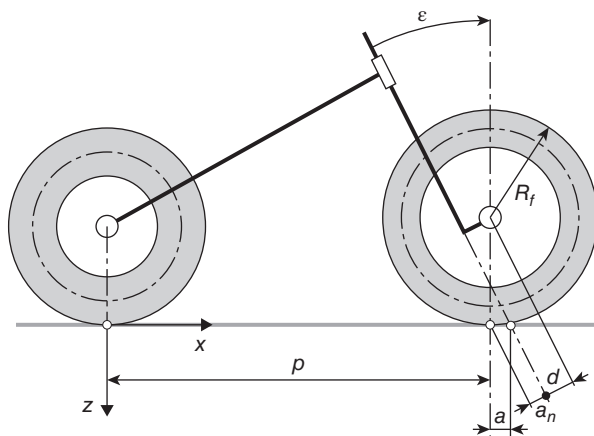

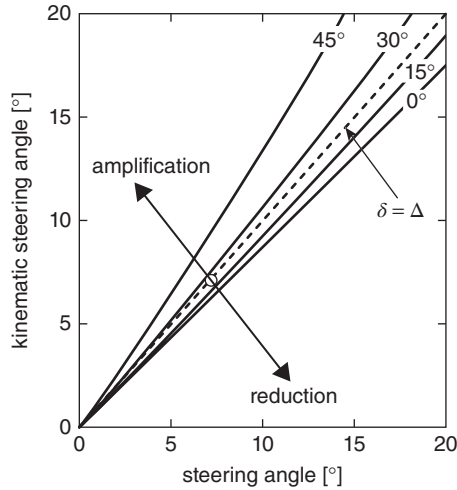**Figure 1.2**   Wheelbase, caster angle and trail

Figure 1.3   Kinematic steering angle Δ as a function of the handlebar steering angle δ for different values of the roll angle ϕ

wheel planes, the so-called kinematic steering angle. In two-wheeled vehicles, the relationship between the handlebar and kinematic steering angles varies appreciably with the roll angle. In particular, the steering mechanism is attenuated (i.e. the kinematic angle is lower than the handlebar angle) up to a certain value of the roll angle (close to the value of the caster angle), then it is amplified (i.e. the kinematic angle is higher than the handlebar angle); see Figure 1.3 for example.

The following simplified expression can be used to estimate the kinematic steering angle Δ from the handlebar steering angle δ, the caster angle ε and the roll angle ϕ:

$$\Delta = \arctan\left(\frac{\cos\varepsilon}{\cos\varphi}\tan\delta\right) \qquad (1.2)$$

The local curvature of the vehicle trajectory C (or the turning radius R_c) can be estimated from the kinematic angle Δ and the wheelbase p using the following expression:

$$C = \frac{1}{R_c} \cong \frac{\tan\Delta}{p} = \frac{\cos\varepsilon}{p\,\cos\varphi}\tan\delta \qquad (1.3)$$

Note that Equation 1.3 does not include the effect of tyre slippage, whose contribution will be described in Sections 1.2 and 1.5.2.

1.2   Tyres

The performance of two-wheeled vehicles is largely influenced by the characteristics of their tyres. Indeed, the control of the vehicle's equilibrium and motion occurs through the generation of longitudinal and lateral forces resulting from the rider's actions on the steering mechanism, throttle and braking system. The peculiarity of motorcycle tyres is that they work with camber angles up to 50° and even more, while car tyres rarely reach 10°.
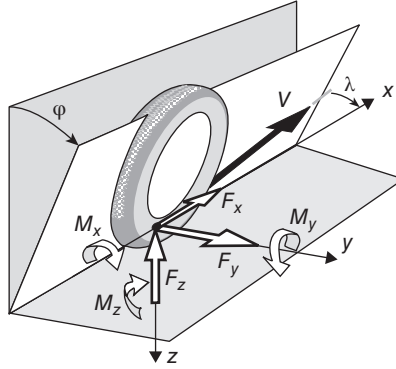
Figure 1.4 Tyre forces and torques

1.2.1 Contact Forces and Torques

From a macroscopic viewpoint, the interaction of the tyre with the road can be represented by a system composed of three forces and three torques, as in Figure 1.4:

- a longitudinal force F_x (positive if driving and negative if braking);
- a lateral force F_y;
- a force F_z normal to the road surface;
- an overturning moment M_x;
- a rolling resistance moment M_y;
- a yawing moment M_z.

Experimental observations show that the force and torque generation is mainly related to the following input quantities:

- tyre longitudinal slip κ;
- tyre lateral slip λ;
- tyre camber angle ϕ;
- tyre radial deflection ζ_R;
- tyre spin rate ω.

Therefore we can write:

$$
\begin{aligned}
F_x &= F_x(\kappa, \lambda, \phi, \zeta_R, \omega) \\
F_y &= F_y(\kappa, \lambda, \phi, \zeta_R, \omega) \\
M_x &= M_x(\kappa, \lambda, \phi, \zeta_R, \omega) \\
M_y &= M_y(\kappa, \lambda, \phi, \zeta_R, \omega) \\
M_z &= M_z(\kappa, \lambda, \phi, \zeta_R, \omega)
\end{aligned}
\tag{1.4}
$$

with the longitudinal force F_x mainly related to longitudinal slip κ, lateral force F_y mainly related to the lateral slip λ and the camber angle ϕ, overturning moment M_x mainly related to the camber angle ϕ, rolling resistance mainly related to the wheel spin rate ω and yawing moment mainly related to the lateral slip λ and camber angle ϕ.
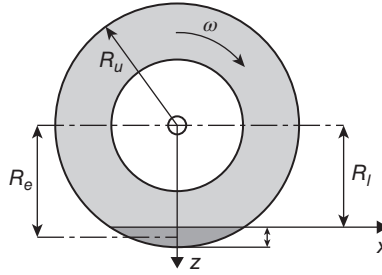
Figure 1.5 Tyre radii

The longitudinal slip (positive when driving and negative when braking) is defined as:

$$\kappa = \frac{\omega R_e - V_x}{V_x},$$ (1.5)

where V_x is the tyre longitudinal velocity, ω is the tyre spin rate and R_e is the tyre effective rolling radius. In particular, the effective rolling radius R_e can be computed from the freely rolling tyre as

$$R_e = V_x/\omega.$$ (1.6)

Note that the effective rolling radius does not coincide with either the tyre loaded radius R_l or the the tyre unloaded radius R_u; see Figure 1.5. This should not be surprising since the tyre is not a rigid body. Experimental observations show that $R_l < R_e < R_u$. However, a common assumption is $R_l = R_e$.

Sometimes a slightly different formulation of longitudinal slip is adopted:

$$\kappa' = \frac{\omega R_e - V_x}{\omega R_e}$$ (1.7)

It can easily be shown that

$$\kappa' = \kappa/(1 + \kappa)$$ (1.8)

and the relative difference between the two is:

$$\varepsilon = (\kappa' - \kappa)/\kappa = -\kappa'$$ (1.9)

which is typically lower than 5% in normal conditions (i.e. no skidding).

The lateral slip is defined as:

$$\lambda = -\arctan\frac{V_y}{V_x}$$ (1.10)

where V_y is the lateral velocity of the tyre and V_x is the longitudinal velocity. The sign is chosen to give positive force for positive slip.

Sometimes another input quantity is considered, the turn slip ϕ_t:

$$\phi_t = -\frac{1}{R_c} = -\frac{\dot{\psi}}{V_x}$$ (1.11)

where R_c is the curvature of the tyre contact point path and $\dot{\psi}$ is the yaw rate. This quantity is important only at very low speed and therefore is not considered in the following sections.

1.2.2 *Steady-State Behaviour*

A widely used model for computing the steady-state tyre forces and moment is based on the so-called Magic Formula (Pacejka 2006). The general form is:

$$y(x) = D\sin[C\arctan\{Bx - E(Bx - \arctan Bx)\}] \tag{1.12}$$

where $y(x)$ passes through the origin $x = y = 0$, reaches a maximum and subsequently tends to a horizontal asymptote; see Figure 1.6. For given values of the coefficients B, C, D, E, the curve shows an anti-symmetric shape with respect to the origin. To allow the curve to have an offset with respect to the origin (e.g. because of ply-steer and conicity of the tyre), two shifts S_H and S_V can be introduced:

$$\begin{aligned} Y &= y(x) + S_V \\ x &= X + S_H \end{aligned} \tag{1.13}$$

Coefficient $D > 0$ represents the peak value of the curve, while the product BCD corresponds to the slope of the curve at the origin (e.g. the lateral slip stiffness when the lateral force is reported in the vertical y axis and the lateral slip is reported in the horizontal x axis). The shape factor $C > 0$ determines the shape of the resulting curve. The factor B is used to determine the slope at the origin and is called the stiffness factor. The factor $E \leq 1$ is introduced to control the curvature at the peak and at the same time the horizontal position of the peak. The various factors depend on the tyre normal load F_z (or tyre radial deflection).

In particular, the slope of the lateral force BCD_y is especially sensitive to load variation, and is usually modelled as follows (Figure 1.7):

$$BCD_y = p_1 \sin(2\arctan(F_z/p_2)) \tag{1.14}$$

The sideslip stiffness attains a maximum p_1 at a normal load $F_z = p_2$.
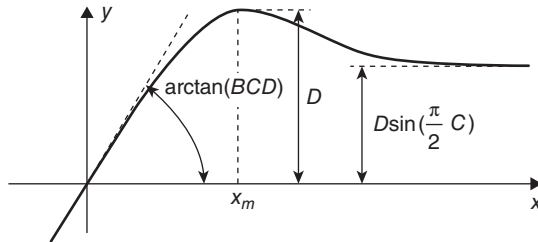

Figure 1.6 Main parameters of the tyre Magic Formula
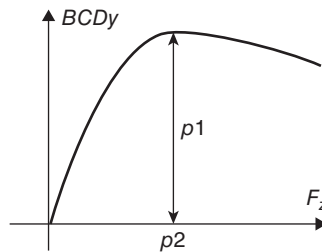

Figure 1.7 Tyre cornering stiffness as a function of normal load

Another widely used tyre formula is the Burckhardt model (Kiencke and Nielsen 2001):

$$y(x) = \vartheta_1(1 - e^{-x\vartheta_2}) - x\vartheta_3 \tag{1.15}$$

Again, the curve typically passes through the origin $x = y = 0$, reaches a maximum and subsequently decreases. An offset can be added, following the same approach used above.

Typical tyre curves are depicted in Figure 1.8.

A fundamental concept when dealing with tyre behaviour is the coupling between longitudinal and lateral forces on the contact patch. In practice, the tyre gives the maximum longitudinal (lateral) force when in pure longitudinal (lateral) slip condition. Indeed, the theoretical analysis on physical models (Pacejka 2006) shows that the tyre longitudinal and lateral force generation depends on the following theoretical slip quantities:

$$\sigma_x = \frac{\kappa}{1 + \kappa} \quad \sigma_y = \frac{\tan \lambda}{1 + \kappa} \tag{1.16}$$

rather than on the practical slip quantities κ and λ, and that there exists a total slip:

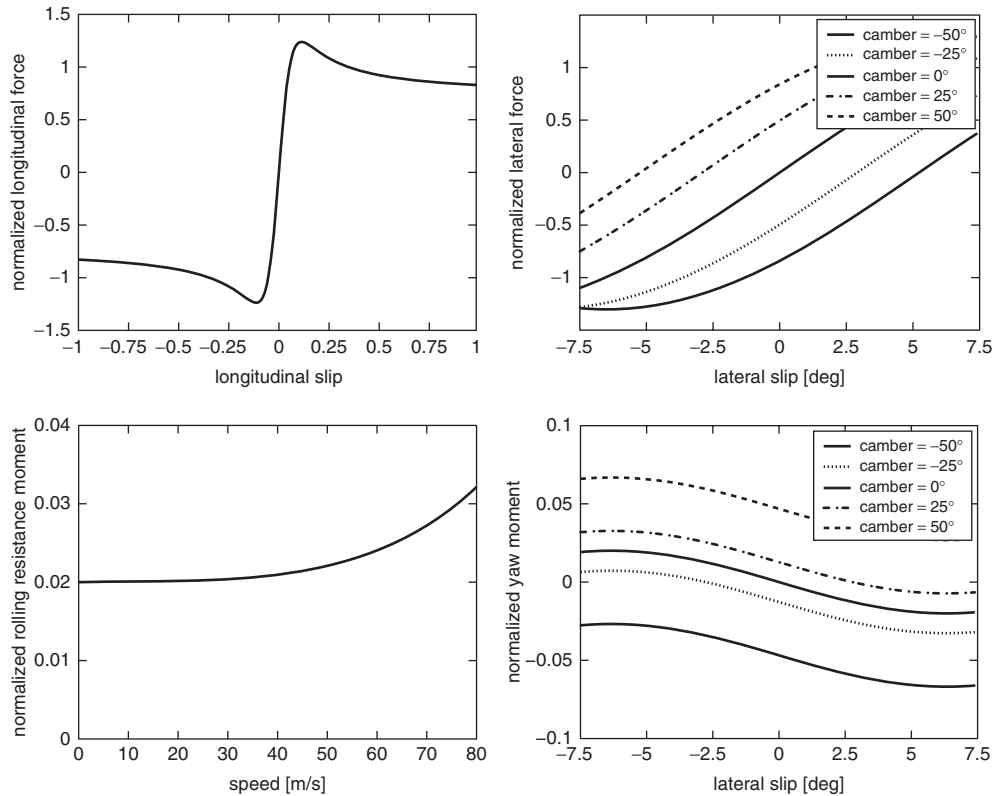$$\sigma = \sqrt{\sigma_x^2 + \sigma_y^2} \tag{1.17}$$

Figure 1.8 Typical tyre curves

which defines the maximum friction force available from the tyre. The corresponding total force can be split between the longitudinal and lateral directions, according to the slip σ_x and σ_y. Also, the effect of camber can be included into the sideslip as follows:

$$\lambda^* = \lambda + \frac{k_\phi}{k_\lambda}\phi \tag{1.18}$$

and the formulas for forces read:

$$F_x = \frac{\sigma_x}{\sigma}F_{x0}(\sigma) \quad F_y = \frac{\sigma_y}{\sigma}F_{y0}(\sigma) \tag{1.19}$$

where F_{x0} and F_{y0} are the longitudinal and lateral forces in pure slip condition.

There is also a newer empirical approach to modelling force coupling (Pacejka 2006). To describe the effect of combined slip on the lateral force and longitudinal force characteristics, the following hill-shaped function G is employed:

$$G = D\cos(C\arctan(Bx)) \tag{1.20}$$

where x is either the longitudinal slip κ or the lateral slip λ (or $\tan\lambda$). The coefficient D is the peak value, C determines the height of the hill's base and B influences the sharpness of the hill, which is the main factor responsible for the shape of the function. The formulas in combined slip conditions read

$$F_x = G_xF_{x0}(\kappa) \quad F_y = G_yF_{y0}(\lambda) \tag{1.21}$$

1.2.3   Dynamic Behaviour

The relationships between the tyre inputs (slips, camber, load/deflection and spin) and the tyre outputs (forces and torques) described in the previous section hold in steady-state conditions. However, the tyre forces do not arise instantaneously: to appear the tyre needs to travel a certain distance, which depends on the tyre characteristics. The physical reason is the tyre flexibility, and the related behaviour can be explained as follows.

We consider a tyre whose contact point has longitudinal velocity $V_x + \dot{\zeta}_x$ and lateral velocity $V_y + \dot{\zeta}_y$, where V_x and V_y are the velocities of the contact point when neglecting tyre deformation, while $\dot{\zeta}_x$ and $\dot{\zeta}_y$ are the deflection velocities; see Figure 1.9.
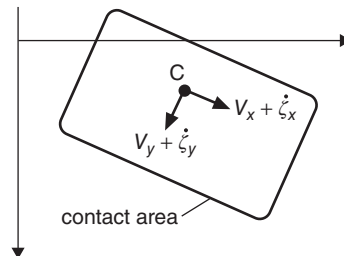

Figure 1.9   Tyre contact area with deflections

The observed longitudinal slip (e.g. with sensors on the rim) is

$$\kappa = \frac{\omega R_e - V_x}{V_x} \tag{1.22}$$

with ω the rim spin rate and R_e the effective rolling radius, while the actual (or instantaneous) longitudinal slip experienced by the contact point is

$$\kappa_i = \frac{\omega R_e - \dot{\zeta}_x - V_x}{V_x} \tag{1.23}$$

and therefore

$$\kappa_i = \kappa - \frac{\dot{\zeta}_x}{V_x} \tag{1.24}$$

Similarly, the observed lateral slip is

$$\lambda = -\arctan\frac{V_y}{V_x}, \tag{1.25}$$

while the actual (or instantaneous) lateral slip is

$$\lambda_i = -\arctan\frac{V_y + \dot{\zeta}_y}{V_x}. \tag{1.26}$$

Under small angle assumption it is

$$\lambda_i = \lambda - \frac{\dot{\zeta}_y}{u} \tag{1.27}$$

At the tyre–road contact point, the slip-induced longitudinal and lateral forces balance the deflection-induced forces. Under small slips assumption the following relationships hold:

$$k_\kappa \kappa_i F_z = k_{\zeta_x} \zeta_x \quad k_\lambda \lambda_i F_z = k_{\zeta_y} \zeta_y \tag{1.28}$$

where k_κ and k_λ are the lateral slip stiffness and longitudinal slip stiffness respectively, k_{ζ_x} and k_{ζ_y} are the lateral and longitudinal structural stiffness and F_z is the tyre normal load. When introducing Equations 1.24 and 1.27 into 1.28 one obtains:

$$k_\kappa \left(\kappa - \frac{\dot{\zeta}_x}{V_x} \right) F_z = k_{\zeta_x} \zeta_x \tag{1.29}$$

$$k_\lambda \left(\lambda - \frac{\dot{\zeta}_y}{V_x} \right) F_z = k_{\zeta_y} \zeta_y \tag{1.30}$$

which yields, after the elimination of carcass deflections ζ_x and ζ_y

$$F_{x0} = \frac{\sigma_\kappa}{u} \dot{F}_x + F_x \tag{1.31}$$

$$F_{y0} = \frac{\sigma_\alpha}{u} \dot{F}_y + F_y \tag{1.32}$$

where F_x and F_y are the actual tyre forces (i.e. computed with the instantaneous slip κ_i and λ_i), while F_{x0} and F_{y0} are the tyre forces computed with the practical slips κ and λ and:

$$\sigma_\kappa = \frac{k_\alpha F_z}{k_{\zeta_x}} \quad \sigma_\alpha = \frac{k_\lambda F_z}{k_{\zeta_y}}. \tag{1.33}$$

In practice, there is a deformation-induced lag between F_x, F_y and F_{x0}, F_{y0}. The resulting first-order differential equations are called *relaxation equations*, with $\sigma_{\kappa,\alpha}$ the relaxation lengths. Equation 1.33 shows that the longitudinal (lateral) relaxation length increases with the longitudinal (lateral) slip stiffness and with the normal load, while it reduces with the longitudinal (lateral) structural stiffness. The relaxation length represents the space that the wheel has to cover in order for the force to be 63% of the steady-state force. Typical values of relaxation length are in the range 0.10–0.4 m, the higher values corresponding to higher tyre normal load and higher speeds.

The equations above describe the effect of flexibilities on the longitudinal force due to longitudinal slip, and lateral force due to lateral slip. Actually, in two-wheeled vehicles there is a significant component of the lateral force related to the camber angle ϕ. Therefore, under small ϕ assumption, Equation 1.28 becomes

$$(k_\lambda \lambda_i + k_\phi \phi) F_z = k_{\zeta_y} \zeta_y \tag{1.34}$$

where k_ϕ is the camber stiffness, and after substitution Equation 1.32 gives

$$F_{y0} + \frac{\sigma_\alpha}{V_x} F_z \dot{\phi} = \frac{\sigma_\alpha}{V_x} \dot{F}_y + F_y. \tag{1.35}$$

Finally, it is worth mentioning the gyroscopic couple that arises as a result of the time rate of change of the tyre camber distortion, the wheel spin rate and the belt inertia. This effect is visible for certain types of tyre at high speeds, and leads to an increase of the observed relaxation length σ_α (De Vries and Pacejka 1998).

1.3   Suspensions

Suspensions serve several purposes such as contributing to the vehicle's road-holding/handling, keeping the rider comfortable and reasonably well isolated from road noise. These goals are generally at odds. In addition, the suspensions affect the vehicle's trim while accelerating, braking, turning and so on. The proper choice of front and rear suspension characteristics depends on many parameters: the weight of the rider and the vehicle, the position of the centre of gravity, the characteristics of stiffness and vertical damping of the tyres, the geometry of the motorcycle, the conditions of use, the road surface, the braking performance, the engine power and the driving technique, among others.

1.3.1   Suspension Forces

The total force F exerted by the spring–damper group is the sum of the following different actions:

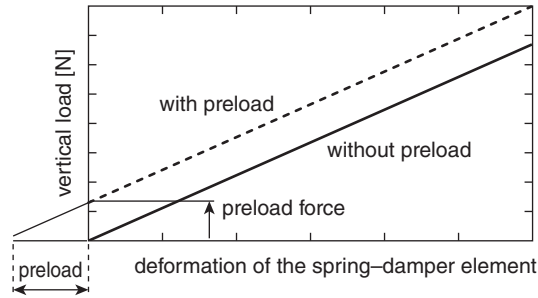$$F = F_e + F_d + F_f + F_p \tag{1.36}$$

Figure 1.10   Elastic force as a function of preload

where F_e is the elastic force exerted by the coil spring and/or air spring (or different elastic components), F_d is the damping force exerted by the shock absorber, F_f is the friction force and F_p is the end-stroke pad force.

  Preloading is commonly used to adjust the initial position of the suspension with the weight of the vehicle and rider acting on it. It consists of a precompression of the spring: as a consequence, if the spring is stressed with forces that are lower than or equal to the preload, it is not compressed. In practice, this adjustment shifts the curve of the elastic force as a function of travel F_e; see Figure 1.10.

1.3.2   Suspensions Layout

Several suspension layouts have been used over the years and the following sections present a brief overview.

1.3.2.1   Front Suspension Types

The most widespread front suspension is the telescopic fork (Figure 1.11a). It is made up of two telescopic sliders which run along the interior of two fork tubes and form a prismatic
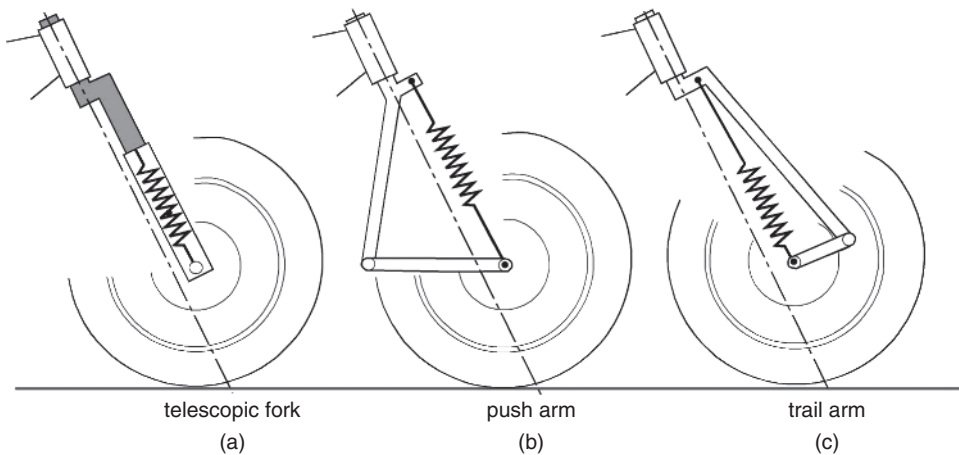

Figure 1.11   Example of front suspensions

joint between the unsprung mass of the front wheel and the sprung mass of the chassis. The telescopic fork is characterized by limited inertia around the axis of the steering head.

Two limitations of the telescopic fork are the impossibility of attaining progressive force displacement and the rather high values of the unsprung mass that is an integral part of the wheel. To overcome the typical defects of the telescopic fork, alternative solutions have been proposed: push arm (Figure 1.11b), trail arm (Figure 1.11c) and four-bar linkage (like the BMW Duolever).

The front arm suspension and four-bar linkage suspensions can be designed so as to present total or partial anti-dive behaviour in braking conditions. Further, the absence of a prismatic joint eliminates the typical dry friction problems of telescopic forks.

1.3.2.2 Rear Suspension Types

The classic rear suspension is composed of a swingarm (a rocker made up of two oscillating arms) with two spring–damper elements, one on each side (Figure 1.12a). The main advantages are the simplicity of construction and the modest reactive forces transmitted to the chassis. Among its disadvantages are a poorly progressive force–displacement characteristic and the possibility that the two spring–damper units generate different forces and therefore torsional stress on the swingarm.

An alternative is represented by the cantilever mono-shock system, characterized by only one spring–damper unit. However, this suspension does not enable a progressive force–displacement characteristic and the positioning of the spring–shock absorber unit close to the engine can cause problems with the absorber's heat dissipation.

The introduction of a four-bar linkage in the rear suspension makes it easier to obtain the desired stiffness curves. Different attachment points of the spring–damper elements can be chosen: for example, in the Kawasaki Uni-Trak the suspension element is between the rocker and the chassis (Figure 1.12b), in the Suzuki Full-Floater it is between the rocker and the swingarm and in the Honda Pro-Link the element is between the connecting rod and the swingarm. Modest unsprung masses are obtained, as well as large wheel amplitude, but langer reactive forces are exchanged between the various parts of the four-bar linkage.

The four-bar linkage (Figure 1.12c) is also the basis of a suspension used especially on the final shaft transmission with universal joints (e.g. the BMW Paralever). The wheel is attached to the connecting rod of the four-bar linkage. The suspension acts as if it were composed of a very long fork fastened to the chassis at the centre of rotation (the point of intersection of the axes of the two rockers). An additional small four-bar linkage can be
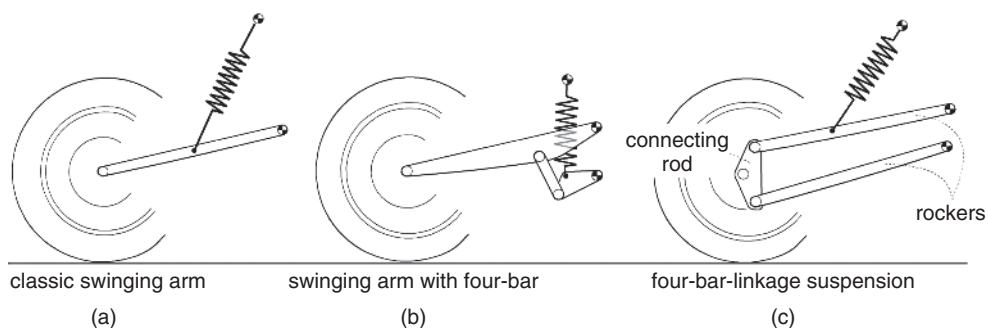

classic swinging arm   swinging arm with four-bar   four-bar-linkage suspension
        (a)   (b)   (c)

Figure 1.12   Example of rear suspensions

added to provide a suitable attachment point for the spring–shock element and thus a proper suspension behaviour.

1.3.3 Equivalent Stiffness and Damping

From a dynamics point of view, the vehicle can be considered as a main sprung body (chassis and rider) connected to two unsprung bodies (wheels) with two elastic systems (front and rear suspension). Also, rather than the characteristics of the spring–damper units, it is important to consider the characteristics of the suspensions in terms of wheel vertical displacement as a function of the vertical force applied. Therefore it is useful to reduce the real suspensions to equivalent, simpler, suspensions represented by two vertical spring–damper elements that connect the unsprung masses to the sprung mass. The parameters defining the equivalent suspension are: reduced stiffness, reduced damping, dependence of the reduced stiffness on the vertical displacement (progressive/regressive suspension), maximum travel and preloading.

To derive the equivalent (or reduced) stiffness, we consider the expression of the variation of the spring force F_e as a function of the travel:

$$F_e = F_0 + k_L(L - L_0) \tag{1.37}$$

where F_0 is the spring force at the initial suspension travel L_0, k_L is the stiffness at L_0 and L is the travel after variation. The power balance between the actual spring force F_e and its equivalent vertical force F_z at the wheel centre is

$$F_z \dot{z} = F_e \dot{L} = F_e \frac{\partial L}{\partial z} \dot{z} \tag{1.38}$$

Therefore

$$F_z = F_e \frac{\partial L}{\partial z} = F_e \tau, \tag{1.39}$$

where τ is the velocity ratio, between the suspension travel velocity and the wheel vertical velocity. The equivalent stiffness k_z is

$$k_z = \frac{\partial F_z}{\partial z} = k_L \tau^2 + F_e \frac{\partial \tau}{\partial z}. \tag{1.40}$$

When assuming a constant velocity ratio the expression simplifies to

$$k_z = k_L \tau^2. \tag{1.41}$$

The derivation of the equivalent (reduced) damping is carried out using the same approach, and therefore Equation 1.40 can also be used for the damping by replacing k_z, k_L with c_z, c_L.

The preload of the equivalent suspension can be computed with the following expression (again from force power balance):

$$F_z|_{L=0} = F_e|_{L=0} \tau \tag{1.42}$$

Finally, the dependence of the reduced stiffness on the vertical displacement can be affected either by changing the characteristic of the velocity ratio τ or by changing the characteristics of the spring element k_L.
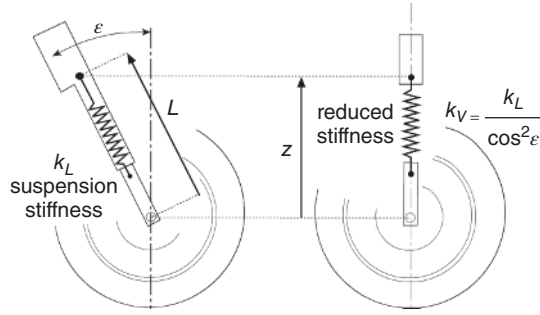
Figure 1.13   Reduced stiffness for the telescopic fork

1.3.3.1   Front

The equivalent stiffness and damping can be easily computed for the widely spread telescopic fork (Figure 1.13). The velocity ratio is derived by considering the geometric relationship between the fork travel and the wheel vertical displacement:

$$\tau = \frac{\partial L}{\partial z} = \frac{1}{\cos(\varepsilon)} \tag{1.43}$$

where ε is the caster angle. Under the assumption of constant stiffness k_L and damping c_L coefficients, and constant velocity ratio τ, the reduced values are

$$k_z = \frac{k_L}{\cos^2\varepsilon} \quad c_z = \frac{c_L}{\cos^2\varepsilon} \tag{1.44}$$

In more complex linkages, the velocity ratio is computed numerically from a kinematic analysis of the mechanism. When it is not constant, or the spring/damper coefficients are not constant, the full Equation 1.40 should be used.

Usually the suspension stiffness k_L is in the range $13-25$ kN/m, and the equivalent stiffness k_z in the range $15-37$ kN/m, while the damping coefficient c_L is in the range $500-2000$ Ns/m, and the equivalent c_z in the range $550-2200$ Ns/m, with the velocity ratio τ in the range $1.05-1.25$ and the caster angle in the range $19-35°$.

1.3.3.2   Rear

The velocity ratio of a rear suspension featuring a linkage depends on many parameters and sometimes cannot be expressed analytically. In any case, the ratio can be easily computed numerically from a kinematic analysis of the mechanism. Typical values of τ for a swingarm with a four-bar linkage are in the range $0.3-0.6$. Usually the suspension stiffness k_L is in the range $100-150$ kN/m, and the equivalent stiffness k_z in the range $10-55$ kN/m, while the damping coefficient c_L is in the range $5-15$ kNs/m and the equivalent c_z in the range $450-5400$ Ns/m.

1.4   In-Plane Dynamics

Vehicle dynamics can be divided between in-plane and out-of-plane dynamics. The former involve the motion of the vehicle in its symmetry plane (e.g. pitch, bounce, suspension travel) and mostly affect the riding comfort and road-holding, while the latter involve the lateral motion of the vehicle (e.g. yaw, roll, steer) and strongly affect the stability and safety. In straight running, two-wheeled vehicles are substantially symmetric and in-plane and out-of-plane motions are decoupled (therefore they can be examined separately), whereas while cornering strong interactions occur.

In this section, different in-plane models of increasing complexity are presented to highlight the main vehicle dynamics involved.

In practice, these dynamics are excited by road undulations and/or by the inertial forces generated while accelerating/braking. Suppose that the vehicle travels with constant velocity V_x on a road with equidistant irregularities (e.g. the bays of a viaduct), Figure 1.14. The time Δt required to cover the distance L between two irregularities (length of the bay) is equal to

$$\Delta t = \frac{L}{V_x} \tag{1.45}$$

and represents the period of the external excitation. A resonance condition occurs whenever the excitation frequency is equal to the natural frequency of one of the in-plane vibration modes of the vehicle. As an example, with $L = 12$ m and $V_x = 24$ m/s, it is $\Delta t = 0.5$ s, so the excitation has a frequency of 2 Hz. In general, several frequency components are present at the same time, depending on the road characteristics.

1.4.1   Pitch, Bounce and Hops Modes

Among the 11 DOFs necessary to fully define the vehicle trim (see Section 1.1), only seven are involved in the in-plane dynamics: longitudinal and vertical motion of the chassis, pitch of the chassis, suspension travel, wheels rotation. If we assume that the vehicle is traveling at constant speed (which is a common assumption when dealing with comfort analysis), the DOFs further reduce to four: vertical motion of the chassis, pitch angle and suspension travel. This DOFs are related to four physical vibration modes: *bounce*, *pitch*, wheel *front hop* and *rear hop*. Bounce is mainly related to the vertical motion of the chassis, pitch is mainly related to the pitch of the chassis and hops are mainly related to the wheels' vertical
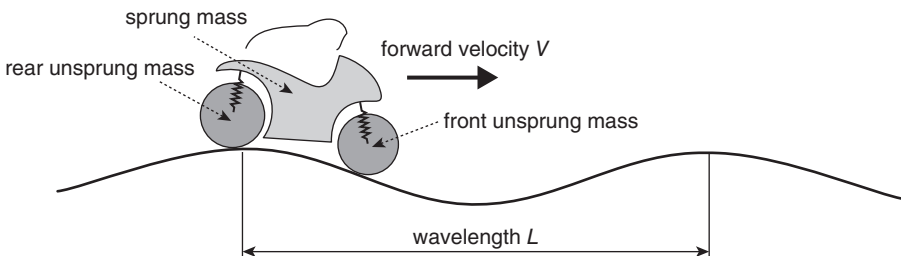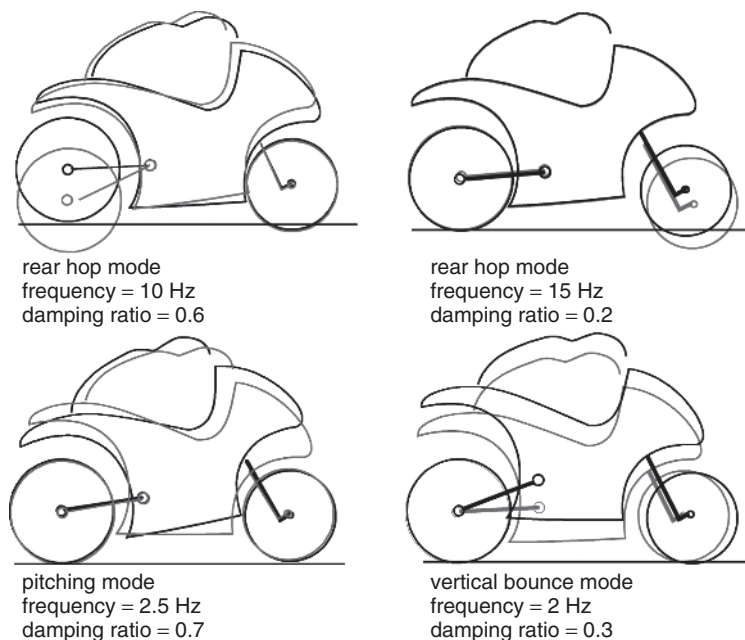

Figure 1.14   Road undulation

Figure 1.15   In-plane vibration modes

motion. In practice, every mode involves some contribution from all four DOFs. Figure 1.15 depicts an example of in-plane vibration modes, with typical values of natural frequency and damping ratio.

In order to model in-plane dynamics, several simple models are commonly used in addition to complex multibody models. The most popular are reported in the following sections.

1.4.1.1   Half-Vehicle Models

The half-vehicle model is a simple yet widespread model used to analyse the suspension–tyre dynamics. The name is due to the fact that only one tyre and one suspension are considered. Two versions are used: one DOF (or SDF) and two DOF.

In the simplest version (Figure 1.16) the model features a mass suspended by a spring–damper element. The mass may represent either the sprung mass (whose share is computed from the whole vehicle mass by considering the tyre loads distribution) or the unsprung mass (wheel rim, brake calliper, etc.). In the former case the spring–damper element represents the suspension, while the tyre compliance is neglected (Figure 1.16a), in the latter case the spring–damper element represents the tyre compliance while the suspension dynamics are neglected (Figure 1.16b). The undamped natural frequency f_0, damped frequency f and damping ratio ζ are

$$f_0 = \frac{1}{2\pi}\sqrt{\frac{k_z}{m}} \quad f = f_0\sqrt{1 - \zeta^2} \quad \zeta = \frac{c_z}{2m(2\pi f_0)} \tag{1.46}$$
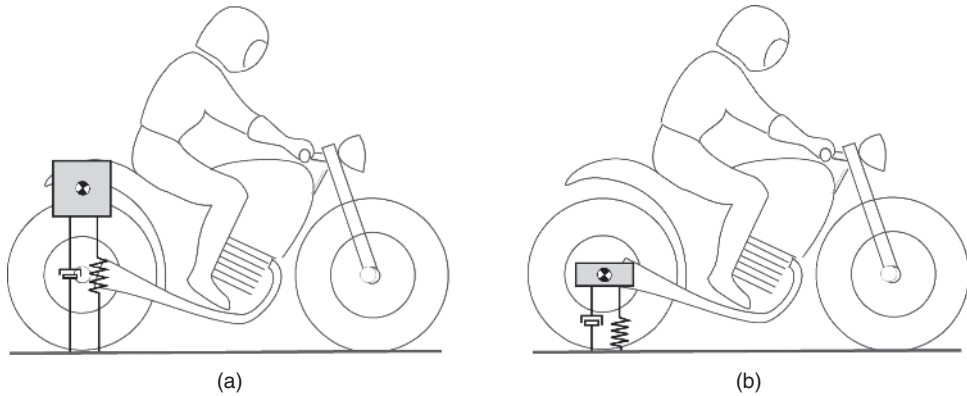
Figure 1.16   Half-vehicle model with (a) one DOF for sprung mass and (b) for unsprung mass

where k_z is the stiffness, c_z the damping coefficient and m the mass. As an example, we consider a vehicle with a mass of 200 kg, including two wheels of mass 15 kg each, a rider with a mass of 80 kg and the whole centre of mass exactly in the middle. We aim at estimating the natural frequency of the front wheel–suspension system, given the front suspension reduced vertical stiffness (see Section 1.3) $k_z = 15$ kN/m and the tyre radial stiffness of $k_T = 180$ kN/m. If we want the model to capture the suspension mode, we use $m = 140$ kg and $k_z = 15$ kN/m, obtaining a natural frequency $f_0 = 1.64$ Hz. Another option is to use a combination of the suspension spring and tyre spring:

$$k_{z'} = \frac{k_z k_T}{k_z + k_T} \tag{1.47}$$

In this case, the stiffness reduces to $k_{z'} = 14$ kN/m and the natural frequency to $f_0 = 1.59$ Hz. Otherwise, if we want the model to capture the wheel hop mode, we use $m = 15$ kg and $k_z = 180$ kN/m, obtaining a natural frequency of 17 Hz.

In the version with two DOFs (Figure 1.17), the model features two masses, representing the sprung mass m_s and unsprung mass m_u, and two spring–damper elements, representing
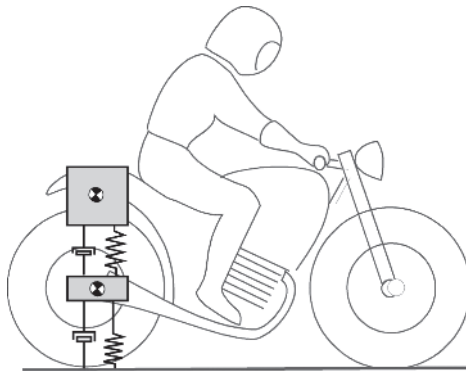

Figure 1.17   Half-vehicle model with two DOFs

the suspension characteristic and the tyre radial compliance. Therefore two modes influencing each other are captured. The expressions for the natural undamped frequencies are:

$$f_{01,02}^2 = \frac{1}{4\pi^2} \frac{-a_1 \pm \sqrt{a_1^2 - 4a_2 a_0}}{2a_2} \tag{1.48}$$

with:

$$a_2 = m_s m_u \qquad a_1 = k_z(m_s + m_u) + k_T m_u \qquad a_0 = k_z k_T. \tag{1.49}$$

Using the vehicle parameters defined above, gives $f_{01} = 1.58$ Hz (suspension mode) and $f_{02} = 18.15$ Hz (wheel hop mode).

1.4.1.2 Full-Vehicle Models

The full-vehicle model has four DOFs and is depicted in Figure 1.18. Since there are no analytic and compact expressions for the system natural frequencies, the equations of motion are reported as:

$$\mathbf{M}\{\ddot{\mathbf{x}}\} + \mathbf{C}\{\dot{\mathbf{x}}\} + \mathbf{K}\{\mathbf{x}\} = \mathbf{0} \tag{1.50}$$

with:

$$\mathbf{x} = \begin{Bmatrix} z \\ \mu \\ z_F \\ z_R \end{Bmatrix} \quad \mathbf{M} = \begin{bmatrix} m & 0 & 0 & 0 \\ 0 & I_{yG} & 0 & 0 \\ 0 & 0 & m_f & 0 \\ 0 & 0 & 0 & m_r \end{bmatrix} \tag{1.51}$$
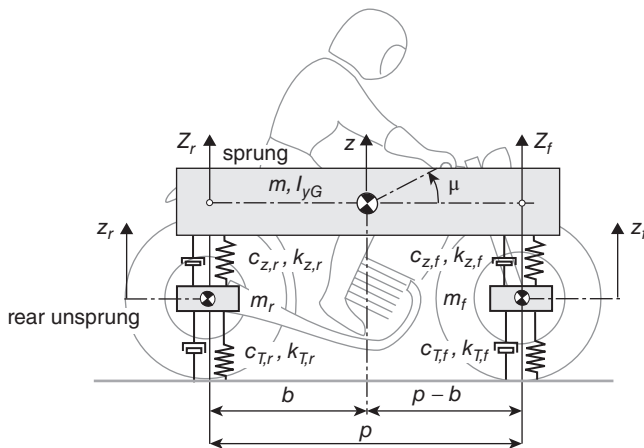

Figure 1.18   Full-vehicle model with four DOFs

$$\mathbf{C} = \begin{bmatrix} c_{z,f} + c_{z,r} & c_{z,f}(p-b) - c_{z,r}b & -c_{z,f} & -c_{z,r} \\ c_{z,f}(p-b) - c_{z,r}b & (p-b)^2 c_{z,f} + c_{z,r}b^2 & -c_{z,f}(p-b) & c_{z,r}b \\ -c_{z,f} & (-p+b)c_{z,f} & c_{z,f} + c_{T,f} & 0 \\ -c_{z,r} & c_{z,r}b & 0 & c_{z,r} + c_{T,r} \end{bmatrix}$$

$$\mathbf{K} = \begin{bmatrix} k_{z,f} + k_{z,r} & -k_{zV,r}b + k_{z,f}(p-b) & -k_{z,f} & -k_{z,r} \\ -k_{z,r}b + k_{z,f}(p-b) & (p-b)^2 k_{z,f} + k_{z,r}b^2 & -k_{z,f}(p-b) & k_{z,r}b \\ -k_{z,f} & (-p+b)k_{z,f} & k_{z,f} + k_{T,f} & 0 \\ -k_{z,r} & k_{z,r}b & 0 & k_{z,r} + k_{T,r} \end{bmatrix}$$

where m_f and m_r are the front and rear unsprung masses respectively, m is the sprung mass, $k_{z,f}$ and $k_{z,r}$ are the front and rear suspension reduced stiffness, $c_{z,f}$ and $c_{z,r}$ are the front and rear suspension reduced damping, $k_{T,f}$ and $k_{T,r}$ are the front and rear tyre radial stiffness and $c_{T,f}$ and $c_{T,r}$ are the front and rear tyre radial damping.

Note that the undamped radian frequencies ω can be numerically derived from

$$|\mathbf{K} - \omega^2 \mathbf{M}| = 0 \tag{1.52}$$

while for the full modal analysis the system must be reduced to a standard first-order formulation before computing the eigenvalues.

1.4.2 Powertrain

Powertrain dynamics involve the fluctuation of the vehicle's longitudinal velocity and wheel rotations, the three DOFs not considered in the models presented in the previous section. Figure 1.19 depicts a common motorcycle powertrain layout, which includes the crankshaft (where the engine propulsive or braking torque is generated), the primary and secondary shafts (whose velocity ratio is set by the rider operating the gearbox lever), the chain final transmission and the rear wheel.
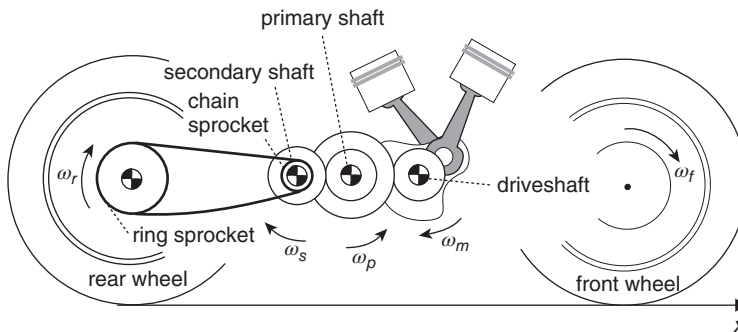

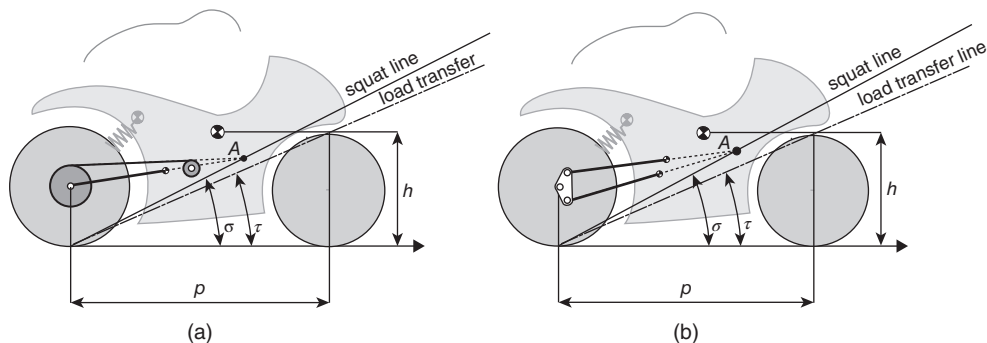**Figure 1.19** Motorcycle powertrain

Figure 1.20 Squat and load transfer lines

It is worth noting that the geometry of the final transmission strongly affects the vehicle trim while varying the propulsive force. In particular, it can be shown (Cossalter 2006) that the variation of the trim of the vehicle rear end (with respect to the standstill configuration) mainly depends on a parameter called the squat ratio R:

$$R = \frac{\tan \tau}{\tan \sigma} \tag{1.53}$$

where τ is the angle of the load transfer line and σ is the angle of the squat line; see Figure 1.20, where the lines are depicted for the swingarm with chain final transmission (Figure 1.20a) and for the four-bar linkage with shaft final transmission (Figure 1.20b).

In more detail, the transfer load line represents the direction of the transfer tyre force acting on the rear contact point. The load transfer is originated by the vehicle acceleration and/or aerodynamic forces. Therefore two transfer lines can be computed: in the case of significant acceleration, the transfer line is the load line, whereas for mild acceleration, the transfer line is the aerodynamic line:

$$\tan \tau = \frac{h_g}{p} \quad \text{or} \quad \tan \tau = \frac{h_a}{p} \tag{1.54}$$

where h_g is the height of the vehicle centre of mass, h_a is the height of the aerodynamic centre and p is the wheelbase.

As regards the squat line, it passes through the rear tyre contact point and the point A, which is the intersection of the swingarm axis with the chain axis, in the case of a final transmission with chain and swingarm (Figure 1.20a), the swingarm pivot on the chassis in the case of a final transmission with shaft and swingarm, and the intersection of the two rockers in the case of a final transmission with shaft and four-bar linkage (Figure 1.20b).

When $R = 1$ (often a design target) there is no variation of the trim of the vehicle rear end while changing the tyre thrust force F_x. In practice, there may be a small variation, due to the theoretical assumptions. When increasing the longitudinal force with $R < 1$ the rear suspension extends, while in the case of $R > 1$ the rear suspension compresses.

1.4.3   Engine-to-Slip Dynamics

The engine torque generated at the crankshaft is transferred through the powertrain to the rear tyre, which generates a longitudinal force as a function of the longitudinal slip. These dynamics are especially important when it comes to the design of traction control systems (Massaro et al. 2011a, 2011b, Corno and Savaresi 2010): three simple models are described below to highlight the physical characteristics of the system.

First we consider a very simple model of the powertrain which does not account for either the tyre or the sprocket absorber flexibilities; see Figure 1.21(a). Note that the sprocket absorber is a device usually placed between the rear wheel sprocket and the rim, with the aim of damping the torsional vibration of the transmission system. This simple model is presented because it is widespread.

The engine torque T is applied to the crankshaft, it is transmitted through the gearbox (according to the selected gear ratio) to the output shaft (whose spin rate is β in Figure 1.21a), it passes through the chain to the rear wheel rim (whose angular velocity is ω) and then to the contact point. The external forces acting on the model are the tyre longitudinal force F_x and the tyre normal load F_z, but rolling resistance is neglected for simplicity. The equation of motion reads:

$$(I_w + I_t)\dot{\omega} = \tau T - R\ F_x \tag{1.55}$$

where I_w is the rear wheel spin inertia, I_t is the transmission inertia reduced to the rear wheel, ω is the spin rate of the wheel rim, τ is the whole transmission ratio, T the engine torque at the crankshaft, R the longitudinal force arm (assumed equal to the rolling radius) and F_x the longitudinal force.

In more detail, the transmission inertia reduced to the rear wheel is computed from the engine spin inertia I_e (plus clutch, starter, etc.), the gearbox primary shaft spin inertia I_p and the gearbox output shaft spin inertia I_o, given the primary ratio τ_p (between the crankshaft and the primary shaft of the gearbox), the gear ratio τ_g (between the primary and the output shaft of the gearbox thus depending on the selected gear) and the final ratio τ_f (between the output shaft and the rear wheel):

$$I_t = ((I_e\tau_p^2 + I_p)\tau_g^2 + I_o)\tau_f^2 \tag{1.56}$$

Moreover the product of the primary ratio, the gearbox ratio and the final ratio is defined as the whole transmission ratio:

$$\tau = \tau_p\tau_g\tau_f \tag{1.57}$$

and represents the ratio between the engine spin rate and the rear wheel spin rate.
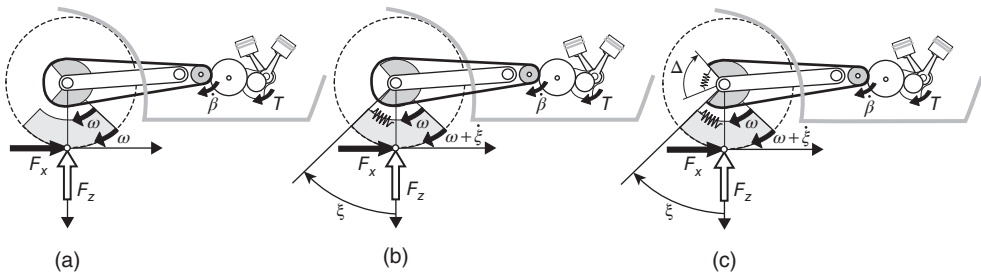

Figure 1.21   Half-vehicle model

For computation of the longitudinal road–tyre force, the full non linear formula is linearized about the steady-state condition (i.e. steady-state longitudinal slip κ_{ss} and steady-state longitudinal force $F_{x,ss}$), thus giving the following relationship between the actual force $F_{x,\kappa}$ and the slip κ:

$$F_{x,\kappa} = F_{x,ss} + k_\kappa(\kappa - \kappa_{ss})F_z \tag{1.58}$$

where k_κ is the slope of the longitudinal slip curve at the linearization point (also called the normalized longitudinal slip stiffness at the linearization point) and F_z is the tyre normal load. The longitudinal slip is defined as:

$$\kappa = \frac{\omega R - V_x}{V_x} \tag{1.59}$$

The model equation can be written in state space formulation:

$$\begin{cases} \dot{\mathbf{x}} = \mathbf{A}\mathbf{x} + \mathbf{B}T \\ \kappa = \mathbf{C}\mathbf{x} \end{cases} \tag{1.60}$$

and the transfer function between engine torque and longitudinal slip can be expressed as:

$$H(s) = \frac{\kappa}{T}(s) = \mathbf{C}(s\mathbf{I} - \mathbf{A})^{-1}\mathbf{B} \tag{1.61}$$

where $\mathbf{I}$ is the identity matrix, s the Laplace variable and:

$$\mathbf{A} = \left[-\frac{R^2 k_\kappa F_z}{(I_w + I_t)V_x} \right] \quad \mathbf{B} = \left[\frac{\tau}{I_w + I_t} \right] \quad \mathbf{C} = \left[\frac{R}{V_x} \right] \quad \mathbf{x} = [\omega]. \tag{1.62}$$

Therefore the system has one pole at:

$$p = -\frac{R^2 k_\kappa F_z}{(I_w + I_t)V_x}. \tag{1.63}$$

Since all the parameters of Equation 1.63 are always positive but k_κ, the plant stability (i.e., the sign of the pole) is bound to the sign of the normalized longitudinal slip stiffness k_κ. In particular, the system is unstable when the slip stiffness k_κ is negative, and this usually happens only for high values of slip (skidding condition), after the peak of the force–slip curve, which usually occurs for slip values in the range 0.1–0.2. Finally, it is worth highlighting that the plant dynamic is very fast at low speeds, $p(V \to 0) = \infty$, and very slow at high speeds, $p(V \to \infty) = 0$.

As a second step, the tyre circumferential compliance is also considered; see Figure 1.21(b). With respect to the previous model, now the rim angular velocity differs from the tyre circumferential angular velocity, because of the deflection ξ. As a consequence, the longitudinal slip expression changes to

$$\kappa_i = \frac{(\omega + \dot{\xi})R - V_x}{V_x}. \tag{1.64}$$

In practice, when it comes to road tests the tyre circumferential deflection is not considered and the slip is computed according to Equation 1.59. For this reason, it is common to refer to Equation 1.59 as practical slip, since this is the slip which is measured in practice, and

to Equation 1.64 as instantaneous slip (Lot 2004), since this is the actual slip at the contact point, which is the physical reason of the tyre longitudinal force. In other words, the instantaneous slip generates the longitudinal force, while the practical slip is what is observed. Therefore, the instantaneous slip κ_i is used to compute the road–tyre force while the practical slip κ is observed when computing the engine-to-slip transfer function Equation 1.61 and when comparing numerical results with road tests. The physical effect of the flexibility is to generate a phase lag between the practical slip and the actual force. Indeed, the actual force is in phase with the instantaneous slip.

A spring–damper element is used to take into account the flexibility of the tyre, and in particular the following expression relates the tyre circumferential deflection ξ and deflection rate $\dot{\xi}$ to the tyre longitudinal force F_x:

$$F_{x,el} = -(k_\xi \xi + c_\xi \dot{\xi})R \tag{1.65}$$

At the contact point, there is force equilibrium between the force due to the elastic deflection $F_{x,el}$ and the force due to the slippage $F_{x,\kappa}$:

$$F_{x,el} = F_{x,\kappa} \tag{1.66}$$

The system now has two equations (1.56 and 1.66) and two state variables (ω and ξ). The following state space matrices are found:

$$\mathbf{A} = \begin{bmatrix} -\dfrac{R^2 k_\kappa N c_\xi}{(I_w + I_t)(k_\kappa N + c_\xi V)} & \dfrac{R^2 k_\kappa N k_\xi}{(I_w + I_t)(k_\kappa N + c_\xi V)} \\ -\dfrac{k_\kappa N}{k_\kappa N + c_\xi V} & -\dfrac{V k_\xi}{k_\kappa N + c_\xi V} \end{bmatrix}$$

$$\mathbf{B} = \begin{bmatrix} \dfrac{\tau}{I_w + I_t} \\ 0 \end{bmatrix} \quad \mathbf{C} = \begin{bmatrix} \dfrac{R}{V} & 0 \end{bmatrix} \quad \mathbf{x} = \begin{bmatrix} \omega \\ \xi \end{bmatrix} \tag{1.67}$$

When inspecting the engine-to-slip transfer function (Equation 1.61), it turns out that at null longitudinal speed the system is vibrating with undamped natural frequency $f_{1,2}$ and damping ratio $\zeta_{1,2}$:

$$f_{1,2} = \frac{1}{2\pi} R \sqrt{\frac{k_\xi}{I_w + I_t}} \quad \zeta_{1,2} = \frac{c_\xi R}{2\sqrt{k_\xi (I_w + I_t)}} \tag{1.68}$$

As the speed increases, the frequency reduces and the damping increases up to a critical velocity (usually in the range 30–60 m/s):

$$V_{cr} = \frac{(c_\xi R + 2\sqrt{k_\xi (I_w + I_t)})F_z k_\kappa R}{k_\xi (I_w + I_t)} \tag{1.69}$$

Above this the system is no longer vibrating (the two poles turn from complex conjugate pairs to real poles).

It is worth noting that there is an alternative approach to account for this tyre force lag. Instead of considering the tyre flexibility, it is possible to add a first-order differential equation (*relaxation equation*, see Section 1.2.3) which replaces Equation 1.66 :

$$\frac{\sigma_\kappa}{V_x}\dot{F}_{x,\kappa} + F_{x,\kappa} = F^0_{x,\kappa} \tag{1.70}$$

where σ_κ is the relaxation length, V_x is the longitudinal velocity, $F_{x,\kappa}$ the actual longitudinal force, $F^0_{x,\kappa}$ the longitudinal force computed with the practical slip of Equation 1.59. The two approaches give similar results when

$$\sigma_\kappa = \frac{k_\kappa F_z}{k_\xi} \tag{1.71}$$

As a third step, a flexible sprocket absorber is introduced between the rear wheel chain sprocket and the rear wheel rim, in addition to the compliant tyre; see Figure 1.21(c). The following expression is used to compute the absorber torque T_a as a function of its deflection Δ:

$$T_a = k_a\Delta + c_a\underline{\Delta} \tag{1.72}$$

where k_a is the absorber stiffness, c_a the damping coefficient and $\underline{\Delta}$ the absorber deflection rate. The state space matrices now read:

$$\mathbf{A} = \begin{bmatrix} -\dfrac{R^2 k_\kappa N c_\xi}{I_w(k_\kappa N + c_\xi V)} & \dfrac{R^2 k_\kappa N k_\xi}{I_w(k_\kappa N + c_\xi V)} & \dfrac{k_a}{I_w} & \dfrac{c_a}{I_w} \\[2mm] -\dfrac{k_\kappa N}{k_\kappa N + c_\xi V} & -\dfrac{V k_\xi}{k_\kappa N + c_\xi V} & 0 & 0 \\[2mm] 0 & 0 & 0 & 1 \\[2mm] \dfrac{R^2 k_\kappa N c_\xi}{I_w(k_\kappa N + c_\xi V)} & -\dfrac{R^2 k_\kappa N k_\xi}{I_w(k_\kappa N + c_\xi V)} & -k_a\left(\dfrac{1}{I_w}+\dfrac{1}{I_t}\right) & -c_a\left(\dfrac{1}{I_w}+\dfrac{1}{I_t}\right) \end{bmatrix}$$

$$\mathbf{B} = \begin{bmatrix} 0 \\ 0 \\ 0 \\ \dfrac{\tau}{I_t} \end{bmatrix} \quad \mathbf{C} = \begin{bmatrix} \dfrac{R}{V} & 0 & 0 & 0 \end{bmatrix} \quad \mathbf{x} = \begin{bmatrix} \omega & \xi & \Delta & \underline{\Delta} \end{bmatrix}^T \tag{1.73}$$

No compact expressions for poles are available, but they can be easily computed numerically from Equation 1.73. The four complex poles of the system are associated with two torsional vibrating modes, which may be either identified in the tyre circumferential and sprocket absorber deflection, or in the wheel and transmission spin.

Finally, it should be noted that when the engine-to-slip dynamics are of interest for frequencies above 30 Hz, the tyre belt dynamics should also be added to the model (thus increasing the number of state variables above four).

1.4.4 Chatter

The chatter of motorcycles is a vibration phenomenon which appears during braking and consists of a vibration of the rear and front unsprung masses with frequency in the range
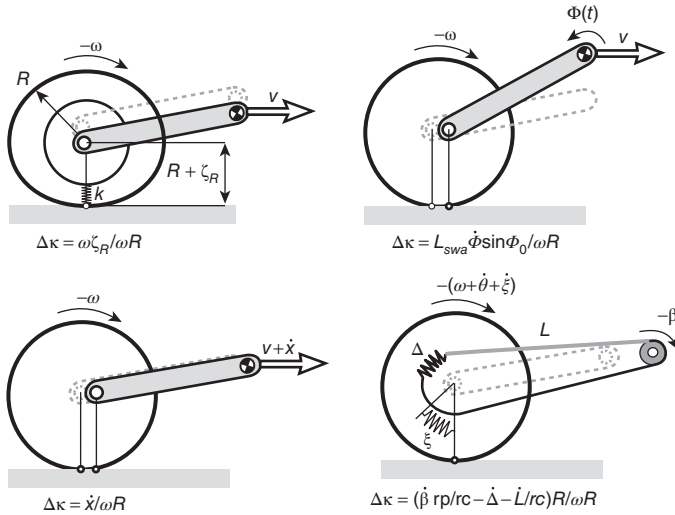
Figure 1.22   Mechanisms generating longitudinal fluctuating slips

17–22 Hz, depending on vehicle characteristics. This vibration could be very strong and acceleration of the unsprung masses can reach 5–10 g (Cossalter et al. 2012, 2008).

A physical explanation of the phenomenon is as follows. The braking manoeuvre may be seen as a composition of two motions: the non-vibrating braking gross motion (i.e. the sequence of equilibrium positions at chosen deceleration and different speeds), and the vibrating motion (i.e. the vehicle oscillation around these equilibrium positions). During braking, the kinetic energy of the gross motion is lost, but if there is an unstable mode part of this energy which is transferred to the in-plane dynamics, so the chatter appears. In practice, when riders start braking there is a transient and the vehicle start vibrating around the equilibrium position. These oscillations lead to a fluctuation of the rear longitudinal slip, i.e. to a variation of the longitudinal force which may drive energy into the system, depending on the phase lag between the rear tyre longitudinal force and fluctuations of the contact point position. The longitudinal slip fluctuations may be grouped into four main origins; see Figure 1.22: a) the radial deflection of the rear tyre ζ_R, b) the fluctuation of the swingarm rotation Φ, c) the fluctuation of the longitudinal speed $\dot{x}$ and d) the fluctuation of the sprocket absorber deflection Δ.

The tyre torsion flexibility and the sprocket absorber flexibility are essential factors to capture the chatter instability, and the chatter vibration depends on the braking style (only front brake, front brake plus rear brake, with or without engine braking, etc.). In more detail, the powertrain flexibility is related to a vibration mode (*transmission* mode) which involves the powertrain inertia and may become unstable under certain motion condition (e.g., while braking with certain deceleration at certain speeds). When inspecting the shape of this vibration mode, components related to the tyre vertical load fluctuation are found, which explain the chattering behaviour.

It is worth stressing that this instability can appear on a perfectly flat road and with perfectly balanced wheels. However, it is expected that both road unevenness and wheel

imbalance can further excite the vibration. In particular, since the wheel spin frequency f_w is:

$$f_w = \frac{V_x}{2\pi R} \tag{1.74}$$

with V_x is the vehicle speed and R the rolling radius, the typical speed range where the road and/or the wheels may further excite the *transmission* mode is 32–42 m/s (115–150 km/h).

1.5   Out-of-Plane Dynamics

Lateral dynamics involve the lateral displacement of the vehicle, yaw, roll and steer angles. In straight running, these dynamics are decoupled from in-plane dynamics, whereas while cornering strong interactions occur. The out-of-plane behaviour has been extensively investigated over the years because it is related to the vehicle stability and safety (Cossalter 2006, 2011b).

In this section, first the two-wheeled steering static response is presented, then the most important vibration modes are discussed.

1.5.1   Roll Equilibrium

The equilibrium roll angle ϕ can be estimated from the curve radius R_c and the vehicle speed V_x as

$$\phi = \arctan \frac{V_x^2}{gR_c}, \tag{1.75}$$

where g is the gravitational acceleration, when considering that the resultant of the centrifugal force and the weight force passes through the line joining the two road–tyre contact points, under the assumption of think-disk tyre, null steering angle and negligible tyre/engine gyroscopic effects. When including the effect of the tyre cross-section, Equation 1.75 changes to (Cossalter 2006):

$$\phi = \arctan \frac{V^2}{gR_c} + \Delta\phi$$
$$\Delta\phi = \arcsin \frac{t \cdot \sin\left(\arctan \frac{V^2}{gR_c}\right)}{h-t} \tag{1.76}$$

which highlights that the actual roll angle increases as the tyre cross-section increases (wide tyre) and the centre of gravity lowers, with t the tyre cross-section and h the height of the centre of gravity; see Figure 1.23.

1.5.2   Motorcycle Countersteering

The lateral dynamics of single-track vehicles is mainly controlled by rider's steering action, even though the rider's body movements can give additional contribution. There is a significant difference when comparing the rider's steering action on a two-wheeled vehicle with that of a driver in a four-wheeled vehicle. In a four-wheeled vehicle the driver turns the steering wheel right (clockwise) to enter a right turn by applying a clockwise steering
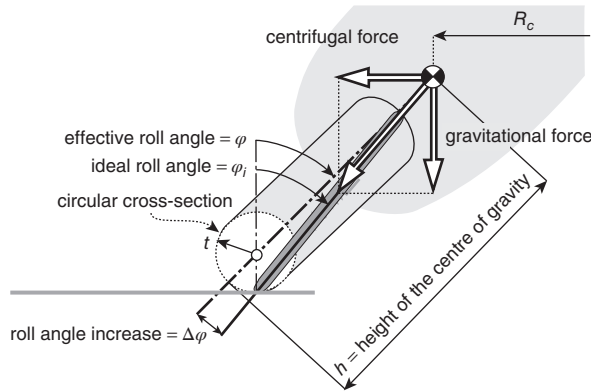
Figure 1.23 Roll equilibrium

torque, and keeps a clockwise steering torque and steering angle all through the turn; however, on a two-wheeled vehicle a completely different approach is used. In order to enter a right turn, the rider has to steer the handlebar angle left (counter-steering manoeuvre) by applying a counter-clockwise steering torque to the handlebar. As a consequence both a centrifugal force on the vehicle and a front tyre lateral force are generated, thus the vehicle leans right into the turn. At this moment, the rider can steer the handlebar into the turn. The final steering torque may be either clockwise or counter-clockwise, depending the vehicle characteristics. The preferred behaviour is to have a counter-clockwise steering torque and a clockwise steering angle when riding a clock wise turn, and motorcycle engineers used to adjust some vehicle parameters to obtain the desired steering torque behaviour.

It is worth noting that the counter-steering manoeuvre can be avoided by using body movement to enter the turn (Bertolazzi et al. 2007). However, steering torque is rather more efficient than body movement torque. Skilled riders take advantage of both mechanisms, while most of the everyday riders ignore the counter-steering approach.

The steering torque applied by the rider to the handlebar is the reaction to the many force contributions (Cossalter et al. 2010). When considering the equilibrium of the front frame in steady-state condition, the rider's steering torque reacts to the forces and torques depicted in Figure 1.24: the tyre longitudinal force, lateral force, vertical load, tyre rolling torque, yawing torque, weight and centrifugal force of the front assembly, and the gyroscopic torque. These contributions can be divided into aligning components and misaligning components. When the aligning components prevail, the rider's handlebar torque is inward to the turn, that is the rider pulls the handlebar with the hand inside the turn. But when the misaligning contributions prevail, the rider's handlebar torque is outward to the turn, that is the rider pushes the handlebar with the hand inside the turn. The tyre lateral force, tyre rolling torque, front frame centrifugal force and wheel gyroscopic effect give self-aligning torques around the steering axis, whereas the tyre longitudinal (braking) force, tyre normal force, tyre yaw torque and front frame weight force give misaligning torques. It is worth noting that in the unusual case where the front frame centre of gravity is behind the steering axis the centrifugal contribution becomes misaligning and the weight contribution aligning. Note that when braking with
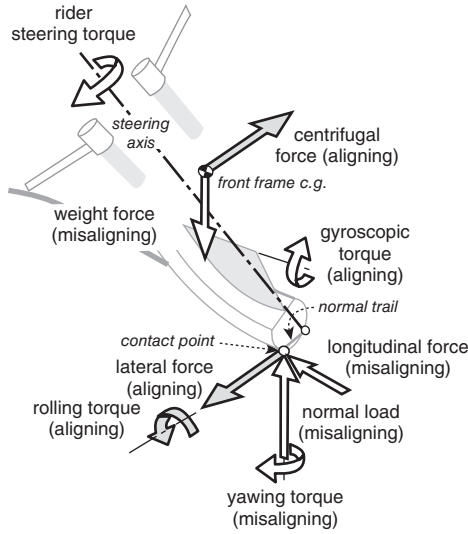
Figure 1.24   Forces and torques acting on the front frame

the front tyre, a significant misaligning component arises, which adds to that related to the longitudinal friction.

The main contributions to the whole steering torque are those related to the tyre normal load and to the tyre lateral force, which almost balance each other. As a consequence of the tyre carcass hysteresis, a rolling torque opposes the wheel rotation and a friction force arises. The longitudinal friction force on the front tyre leads to a small misaligning contribution to the steering torque, whose presence is due to the fact that the tyre carcass is not a thin disk, and therefore the longitudinal force has a non-null component when the vehicle is leaned because of the migration of the contact point on the tyre carcass. The tyre rolling torque also gives an (aligning) contribution to the steering torque related to the fact that when the vehicle is leaned, the rolling torque projection on the steering axis is no longer null. Another important contribution is that related to the tyre yaw torque. This contribution to the steering torque is always misaligning and significant. The gyroscopic contribution (always aligning) to the steering torque arises because the front wheel is both rolling about its spin axis and yawing as a consequence of the cornering manoeuvre. Finally, minor components are those related to the front frame weight (misaligning), and to the front frame centrifugal effect (aligning).

1.5.2.1   Understeering and Oversteering

The steering behaviour of the vehicle depends on many parameters, and in particular on the tyre properties. Indeed, when considering tyres slippage, the effective steering angle becomes (Figure 1.25):

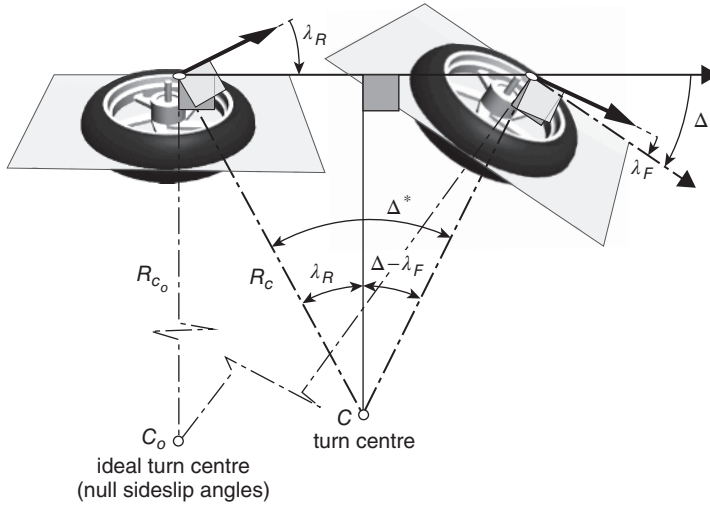$$\Delta^* = \Delta + \lambda_R + \lambda_F \tag{1.77}$$

Figure 1.25   Kinematic steering angle Δ and effective steering angle Δ^*

with Δ from Equation 1.2, λ_R the rear tyre sideslip angle and λ_F the front tyre sideslip angle. In practice, the effective steering angle Δ^* is equal to the kinematic steering angle Δ only when both tyres have the same sideslip, that is $\lambda_R = \lambda_F$ (or when there is no sideslip, which is a reasonable assumption at very low speeds). Otherwise, it is smaller or larger, giving an understeering or oversteering behaviour respectively.

The steering behaviour can be expressed by means of the steering ratio ξ:

$$\xi = \frac{R_{c0}}{R_c} = \frac{\Delta^*}{\Delta} \approx 1 + \frac{\lambda_r - \lambda_f}{\Delta} \tag{1.78}$$

where R_{c0} is the kinematic radius of curvature and R_c is the actual radius of curvature.

The vehicle's steering behaviour can be defined as follows:

- neutral: $\xi = 1 \Longleftrightarrow \lambda_R = \lambda_F$;
- oversteering: $\xi > 1 \Longleftrightarrow \lambda_R > \lambda_F$;
- understeering: $\xi < 1 \Longleftrightarrow \lambda_R < \lambda_F$.

In case of oversteering vehicles, there may be a critical speed V_{cr} where $\Delta = 0$ and therefore $\xi \to \infty$. Above this speed the vehicle is ridden in counter-steering, i.e. the rider has to keep the handlebar turned outside the turn (as in speedway races).

Unlike in four-wheeled vehicles, considerable camber angles (up to 50–60°) are present while cornering with two-wheeled vehicles. Therefore the steering ratio is also significantly affected by the characteristics of the lateral force as a function of camber (in addition to the characteristics of the force as a function of lateral slip). This can be effectively highlighted when expressing the steering ratio for a simple vehicle model under the assumption of small roll angles and linear tyre behaviour:

$$F_{y,R} = (k_{\lambda,R}\lambda_R + k_{\phi,R}\phi_F)F_{z,R} \quad F_{y,F} = (k_{\lambda,F}\lambda_F + k_{\phi,F}\phi_F)F_{z,F} \tag{1.79}$$

where $F_{y,R}$ and $F_{y,F}$ are the rear and front tyre lateral forces respectively, $k_{\lambda,R}$ and $k_{\lambda,F}$ are the rear and front sideslip stiffnesses, $k_{\phi,R}$ and $k_{\phi,F}$ are the rear and front tyre camber stiffnesses, λ_R and λ_F are the rear and front sideslip angles ϕ_R and ϕ_F are the rear and front tyre camber angles and $F_{z,R}$ and $F_{z,F}$ are the rear and front tyre normal loads. Solving Equation 1.79 for the sideslip angles gives:

$$\lambda_R = \frac{1}{k_{\lambda_R}}\left(\frac{F_{y,R}}{F_{z,R}} - k_{\varphi_R}\varphi_R\right) \quad \lambda_F = \frac{1}{k_{\lambda_F}}\left(\frac{F_{y,F}}{F_{z,F}} - k_{\varphi_F}\varphi_F\right) \tag{1.80}$$

In steady turning, under the assumption of small camber angles, we have

$$\frac{F_{y,R}}{F_{z,R}} \approx \phi_R \approx \phi_F \approx \frac{F_{y,F}}{F_{z,F}} \tag{1.81}$$

which can be used in Equation 1.80 to give

$$\lambda_R \approx \frac{1 - k_{\varphi_R}}{k_{\lambda_R}}\varphi \quad \lambda_F \approx \frac{1 - k_{\varphi_F}}{k_{\lambda_F}}\varphi \tag{1.82}$$

When using Equation 1.82 in Equation 1.78, the steering ratio becomes

$$\xi = \frac{1}{1 - \left(\frac{1-k_{\varphi_R}}{k_{\lambda_R}} - \frac{1-k_{\varphi_F}}{k_{\lambda_F}}\right)\frac{V_x^2}{gR}} \tag{1.83}$$

which shows that it is possible to mitigate the oversteering behaviour by increasing the rear tyre camber stiffness and reducing the front tyre camber stiffness, as well as increasing the rear tyre sideslip stiffness and reducing the front tyre sideslip stiffness.

Finally, note that other authors define the steering behaviour differently, using the variation of the steering ratio (as a function of the vehicle speed V_x while travelling on a curve with constant radius R_c) rather than its absolute value:

- neutral: $\left(\frac{\partial \xi}{\partial V}\right)_{R_c} = 1$;
- oversteering: $\left(\frac{\partial \xi}{\partial V}\right)_{R_c} > 1$;
- understeering: $\left(\frac{\partial \xi}{\partial V}\right)_{R_c} < 1$.

With this latter definition, there may be oversteering also with $\lambda_R < \lambda_F$, where the previous definition defines understeering. In practice, we define oversteering as a condition where, on a steady turn, the rear tyre sideslip increases more than the front sideslip when increasing the vehicle speed.

1.5.3 Weave, Wobble and Capsize

In straight motion out-of-plane dynamics involves four of the eleven DOFs necessary to fully define the vehicle trim (see Section 1.1): the lateral displacement of the vehicle, the yaw, roll and steer angles. These DOFs combine to give three well-known vibration modes: *capsize*, *weave* and *wobble*.
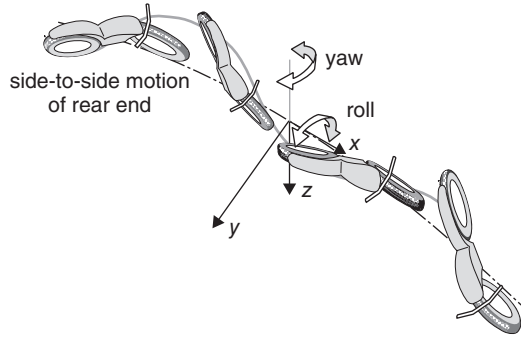
Figure 1.26   Weave mode

Capsize is a non-vibrating mode which mainly consists of a roll motion combined with a lateral displacement (plus some less important steering and yaw movements). Depending on the vehicle characteristics it can be stable at low speeds, then slightly unstable above a critical speed, or slightly unstable over the whole speed range. In any case, this mode is easily controlled by rider.

Weave is an oscillation of the entire motorcycle (Figure 1.26), with frequency rising with speed from 0 up to 3–4 Hz depending on the vehicle characteristics. It is usually unstable for speeds up to 6–7 m/s, then it is stable and tends to be poorly damped at high speeds (>100 km/h or 28 m/s). High speed instability may occur both hands-off or hands-on the handlebars, with the former having the potential to be more stable than the latter under the same set of running conditions (Massaro et al. 2012). More precisely, at zero speed the weave consists of two non-vibrating modes: *body capsize* and *steering capsize*. These two modes coalesce to generate the vibrating weave at a speed in the range 0–1 m/s.

Body capsize is a capsize of the whole vehicle an inverted pendulum-like roll instability. Its time constant τ_{bc} can be estimated with a simple inverted pendulum model:

$$\tau_{bc} = \sqrt{\frac{I_x + Mh^2}{Mgh}} \tag{1.84}$$

where I_x is the whole vehicle moment of inertia around the centre of mass, M is the whole vehicle mass, h is the height of the vehicle centre of mass and g is the gravitational acceleration.

Steering capsize is a steering instability, due to the misaligning effects of both the front frame mass and the front tyre normal load. Its time constant can be estimated with a simple front frame model:

$$\tau_{sc} = \sqrt{\frac{(M_f g b_f + F_{z,f}\, a_n)\sin\varepsilon}{I_f}} \tag{1.85}$$

where M_f is the front frame mass, b_f is the distance of the front frame centre of mass from the steering axis, $F_{z,f}$ is the front tyre normal load, a_n is the normal trail and ε is the caster angle.
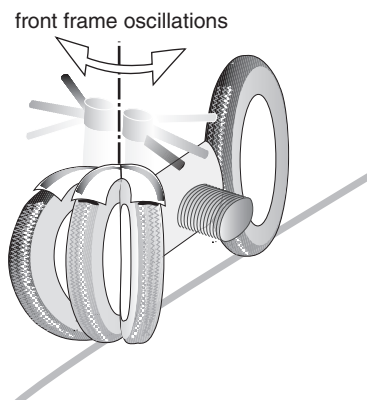
Figure 1.27   Wobble mode

Finally, *wobble* is a vibrational mode dominated by the oscillation of the front steering assembly around the steering axis (Figure 1.27) in the range 6–10 Hz. In practice, wobble mode is usually visible with hands off the handlebars (Cossalter et al. 2007b) and, depending on front assembly structural compliance and wheel imbalance, may become perceptible to the rider at low to medium speeds.

Summarizing, the typical stability behaviour of a motorcycle at constant speed in straight line motion is the following. At standstill, the vehicle is unstable because of body capsize and steering capsize. Indeed, riders put their feet on the road to prevent the vehicle from falling over. For speeds up to 6–7 m/s the motorcycle is unstable because of weave mode and therefore a rider action is needed to stabilize the vehicle. Above 6–7 m/s the vehicle enters a self-stabilizing zone, so no rider action is necessary to stabilize the system (the two-wheeled vehicle also keeps upright with the rider's hands off the handlebars). At increasing speeds, the capsize may become slightly unstable (with hands off the handlebar), but this instability is easily stabilized by rider's passive action on the handlebars. If the vehicle has been properly designed, there should not be any weave or wobble instability in normal riding conditions. However, high speed and cargo loading promote poorly damped weave while wobble may be triggered by wheel imbalance and certain road surfaces. Moreover, these two vibration modes are dangerous because riders may have difficulty in controlling them. In addition, most of the parameters improving the stability of one, worsen the other. This is why their behaviour must be carefully considered when designing the vehicle.

1.5.3.1   Rigid Bodies Model

In this section the results of a basic model made of rigid bodies are presented to discuss the lateral vibration modes of the vehicle (*www.multibody.net*). Since the aim is to study the stability in straight motion at constant speed, the presence of the suspensions can be neglected and only four DOFs are required: lateral displacement y, yaw angle ψ, roll angle ϕ and steering angle δ. Moreover, the tyre properties can be linearized, since only small lateral slips and the roll angle will be employed by a vehicle vibrating around the upright trim. Tyre pure rolling can be assumed in the longitudinal direction, since there is no interest

in the longitudinal dynamics. The effect of tyre flexibility (and the related force lag, see Section 1.2.3) is accounted for by including in the model the front and rear tyre lateral deflection ζ_R and ζ_F. Note that the non-instantaneous tyre behaviour is essential for capturing wobble. The only rider input is the steering torque τ. The model has four rigid bodies: the rear frame (including rider and swingarm), the front frame (handlebar and suspension) and wheels. Its equations of motion can be written in state space form:

$$\dot{\mathbf{x}} = \mathbf{A}\mathbf{x} + \mathbf{B}\mathbf{u}$$
$$\mathbf{x} = \{\underline{y}, \psi, \underline{\psi}, \phi, \underline{\phi}, \delta, \underline{\delta}, \zeta_R, \zeta_F\}^T$$
$$\mathbf{u} = \{\tau\}$$

(1.86)

where y, ψ, ϕ, δ represent the derivatives of the corresponding variables.

The stability is analysed by computing the eigenvalues of $\mathbf{A}$ in Equation 1.86 at different speeds, see the dotted lines of Figure 1.28. The hands-off vehicle stability reads as follows. Up to a speed of 0.6 m/s the vehicle is unstable because of both body capsize (real positive eigenvalue with time constant 0.30 s at 0.1 m/s) and steering capsize (real positive eigenvalue with time constant 0.17 s at 0.1 m/s). At 0.6 m/s the two unstable modes coalesce to give the unstable weave (complex conjugate pair eigenvalues), whose frequency rises from 0 at 0.6 m/s to 0.4 Hz at 7 m/s. From here on the weave is stable and its frequency rises with speed (3 Hz at 40 m/s). Note that at high speeds the mode moves towards the instability area. Wobble has a frequency in the range 7–8 Hz and is unstable for speeds higher than 22 m/s. Capsize is stable in the whole speed range. There is also another mode, usually called rear wobble or weave 2: it is vibrating for speeds up to 25 m/s, then it splits into two non-vibrating modes. This mode is not very interesting because it is very stable over the whole speed range, and therefore is not shown in Figure 1.28.
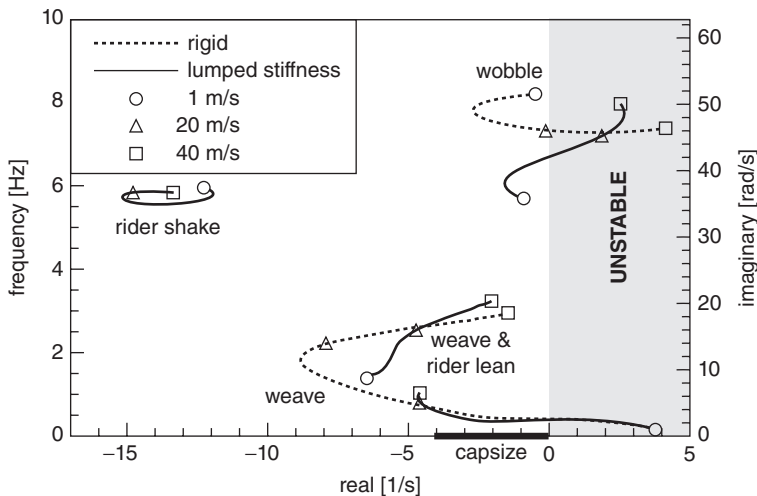

Figure 1.28   Example of motorcycle root-locus as a function of speed

1.5.3.2 Effect of the Frame Compliance

The frame compliance and rider passive mobility can significantly affect the stability of two-wheeled vehicles (Cossalter et al. 2007b) includes an experimental validation). In particular, the most important structural flexibility is that of the front assembly with respect to the rear assembly, while the rider passive roll vibration is the most important rider passive motion affecting stability.

The model used in the previous section is extended to include the main vehicle compliance (the equations and state matrices are reported at *www.multibody.net*). In particular, several DOFs are added to account for: swingarm torsion and bending flexibility (α_R and β_R), front frame bending and torsion flexibility (α_F and β_F) and rider lateral and roll passive motion on the saddle (y_p and ϕ_p). The motion along these new DOFs is restrained by means of spring–damper elements tuned to replicate the real vehicle compliance properties. The additional DOFs are related to the same number of complex conjugate pairs representing the structural modes of vibration. Even more important, these DOFs enter the weave and wobble which affects their stability.

In particular, the front frame bending strongly affects the *wobble* stability (Figure 1.29). The rigid vehicle model predicts a stable wobble at low speeds (up to 22 m/s in the vehicle considered here) and unstable wobble at high speeds, but when including the front flexibility the model predicts an instable vibration mode at low speeds and a stable mode at high speeds. In other words, the front frame flexibility reverses the behaviour of wobble stability as a function of speed. The physical reason of the stabilization effect is the additional gyroscopic effect generated by the deflection rate combining with the wheel spin inertia and spin rate (Cossalter et al. 2007b).

The effect of swingarm bending and torsion flexibility on weave stability is depicted in Figures 1.30 and 1.31 respectively. In the vehicle analysed, the bending has a negligible to positive effect on high speed weave stability (again the stabilizing effect is related to the additional gyroscopic effect induced by bending deflection), while the torsion flexibility worsens the high speed weave stability.
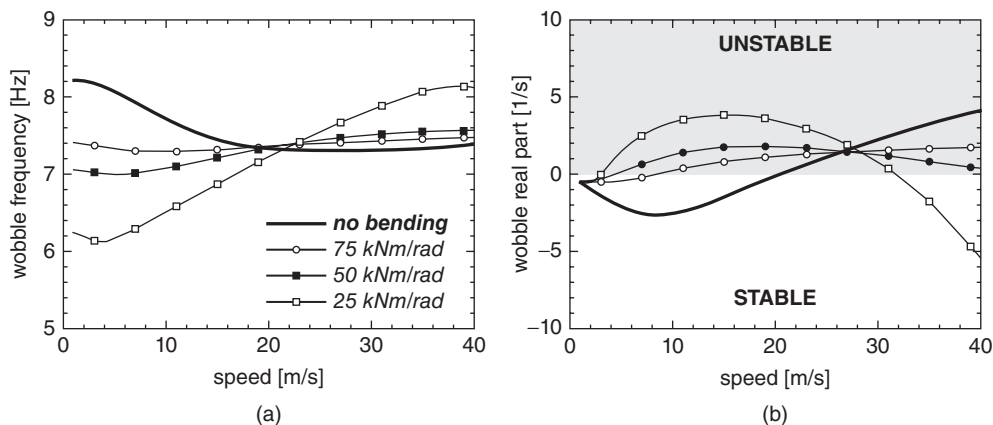

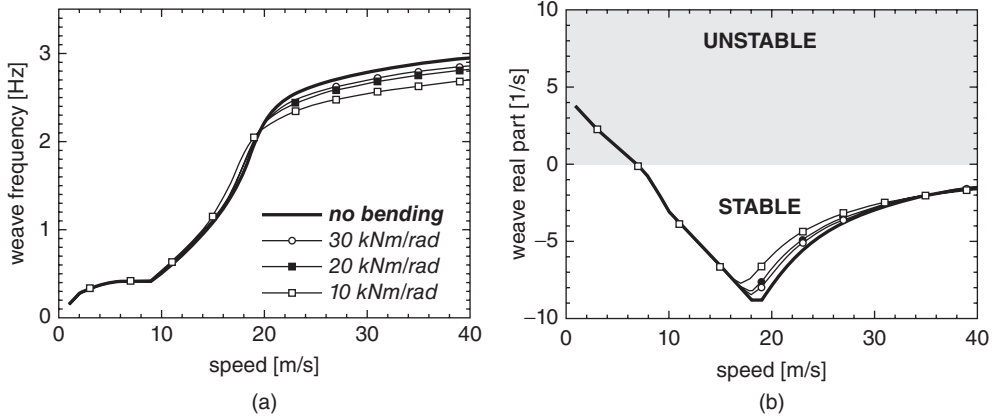**Figure 1.29** Effect of front bending on wobble

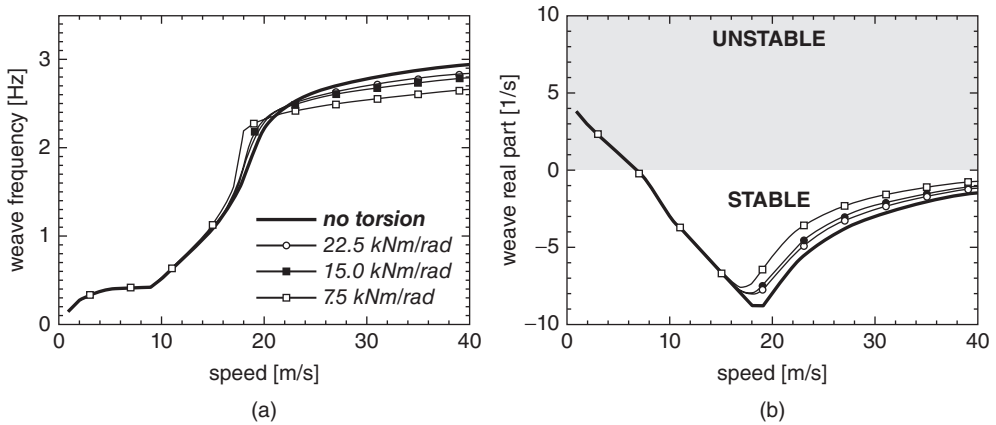**Figure 1.30**   Effect of rear bending on weave

Figure 1.31   Effect of rear torsion on weave

The effect of the rider's passive motion has been considered by allowing the rider to vibrate on the saddle. The rider's body is split into a lower body (from feet to hip) and an upper body (from hip to head). The lower body is allowed to move laterally with respect to the rear frame, while the upper body is allowed to roll with respect to the lower, around a roll axis passing in the neighbourhood of the rider's hip. The rider's motion is restrained by spring–damper elements tuned to give the typical rider modal characteristics (the lateral natural frequency is usually in the range 3.5–4.0 Hz with damping ratio in the range 0.3–0.6, while the roll natural frequency is in the range 0.8–1.5 Hz and damping ratio 0.1–0.3 (Nishimi et al. 1985, Katayama et al. 1987). The rider's passive motion is included in the model, and its stability is compared with the case with rigid bodies in Figure 1.28, where the continuous lines represent the model with the compliant bodies and the rider's motion, while the dotted lines represent the model with rigid bodies. The rider's lateral motion is related to a new

vibration mode named *rider shake* while the roll motion deeply merges with the weave, whose curve is now split. In practice, the rider's motion stabilizes the wobble at low speed and significantly stabilizes the high speed weave, since the effect of roll on weave is the more important contribution.

When accelerating, the weave mode tends to increase its frequency while that of the wobble reduces, and a coupling between them may also take place. When braking, the wobble mode increases its frequency and usually reduces its damping while the weave reduces its frequency and damping. It is worth stressing that all the considerations reported in this section refers to the free vehicle stability, that is, they remain valid when the rider has hands off the handlebar or gently grasping the handlebar (Massaro et al. 2012).

1.5.3.3   Effect of the Rider Impedance

In practice, the rider has their hands on the handlebar while riding the vehicle. This may change the two-wheeled vehicle stability because of the loop created between the rider's body, the rear frame (where the rider sits) and the front frame (where the rider's hands are). The effect of such rider passive steering impedance on vehicle stability has only recently been investigated (Sharp and Limebeer 2004, Cossalter et al. 2011a, Massaro and Cole 2012, Massaro et al. 2012, with only the last including a comparison with experimental road tests).

To model this effect, the rider's upper body is allowed to yaw with respect to their lower body and the handlebar. The motion is restrained by spring–damper elements properly tuned to give the experimentally measured rider's modal properties, Figure 1.32.

The effect of rider impedance is to stabilize the wobble mode and to destabilize the high speed weave mode. The effect is similar to that of a steering damper. However, while an ideal steering damper generates a steering torque τ proportional to and in phase with the
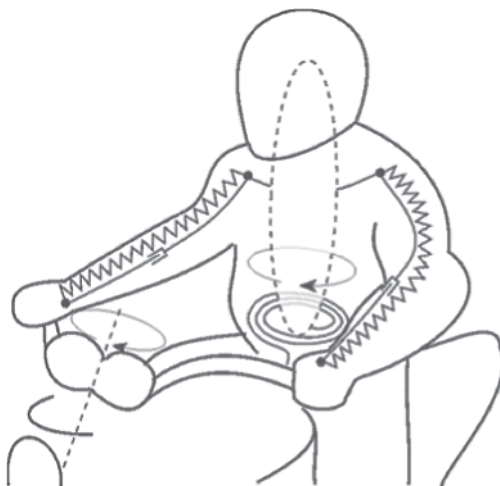

Figure 1.32   Rider impedance model

steering angle rate $\dot{\delta}$:

$$\tau = c_d \dot{\delta} \tag{1.87}$$

the steering torque generated by the rider changes with frequency, both in magnitude and in phase. Moreover, while the steering damper generates equal and opposite torques on the front assembly and on the rear assembly, the rider does it only at low and high frequency, because of the presence of the inertia.

1.6   In-Plane and Out-of-Plane Coupled Dynamics

In the previous two sections in-plane and out-of-plane dynamics have been treated separately, using simplified models in order to highlight the most important vehicle behaviour. However there are conditions (e.g. entering a curve while braking, Massaro 2011, Massaro and Lot 2010) where it is essential to capture the coupling between in-plane and out-of-plane dynamics using full vehicle models like *FastBike* (Cossalter et al. 2011b; Cossalter et al. 2011c). Below three typical examples of coupled dynamics are reported.

Cornering Stability

When cornering, the in-plane and out-of-plane dynamics couple (Cossalter et al. 2004) and all the vehicle vibration modes include both in-plane and out-of-plane DOFs. The interactions may be predicted from straight line motion stability, when in-plane and out-of-plane modes have eigenvalues close to each other in the root locus. A typical coupling is between *bounce/pitch* and *weave*: in this condition also the set-up of the suspension can be used to control the cornering oscillations. Similarly, *wobble* may combine with wheel *front hop* mode, to give a steering oscillation combined with the suspension oscillation.

It is also important to highlight that, while in straight line motion the in-plane modes are almost speed independent, while in cornering all the modes depend on the speed of travel.

Kick Back

Road undulations or transverse joints, such as on motorway bridges, may unload the front wheel of the vehicle, which lifts up from the road surface. The rider usually reacts automatically with a steering action bringing the front wheel plane out of the driving direction of the bike. When the front wheel makes contact with the road surface again, the front frame is not in force equilibrium with respect the steering axis. As a consequence an impulsive force is generated, which 'kicks back' the front frame opposite to the direction of the steering angle (Lot and Massaro 2007). The kick back phenomenon can be so heavy that the rider cannot control the handlebar and consequently loses control of the motorcycle. The steering angle can reach very high values. This phenomenon may appear both in straight-running (especially when accelerating) or while cornering. It is worth noting that it is not related to a new vibration mode, but to the stability of weave and wobble modes. In practice, the less stable mode is the most excited and therefore the resulting vibration may either be in the wobble or in the weave frequency range.

High Side

This phenomenon is due to the interaction between the rear tyre lateral force and the longitudinal force. It can happen during a braking manoeuvre while entering a curve or during a thrusting manoeuvre while exiting from a curve (Cossalter et al. 2007a).

For example, to exit the curve the rider starts to thrust the rear wheel, therefore the longitudinal driving force increases and adds to the existing lateral force. If the total tyre friction force reaches the limit value, the rear wheel loses grip and therefore the rear of the motorcycle moves outwards from the turn. The rider reacts by reducing the throttle opening, so the thrust force reduces suddenly, and the rear tyre regains its grip. The existing large sideslip (originated by the earlier grip loss), generates a lateral force impulse that violently pushes the motorcycle upwards and may even throw the rider out of the saddle. In any case, weave mode is strongly excited by the impulse action.

References

Bertolazzi E, Biral F, Da Lio M and Cossalter V 2007 The influence of riders upper body motions on motorcycle minimum time maneuvering *Multibody Dynamics 2007, ECCOMAS Thematic Conference*.

Corno M and Savaresi S 2010 Experimental identification of engine-to-slip dynamics for traction control applications in a sport motorbike. *European Journal of Control* **16**(1), 88–108.

Cossalter V 2006 *Motorcycle Dynamics*. Lulu.

Cossalter V, Aguggiaro A, Debus D, Bellati A and Ambrogi A 2007a Real cases motorcycle and rider race data investigation: fall behavior analysis *20th International Technical Conference on Enhanced Safety of Vehicles: Innovations for Safety Opportunities and Challenges*.

Cossalter V, Doria A, Lot R and Massaro M 2011a The effect of rider's passive steering impedance on motorcycle stability: Identification and analysis. *Meccanica* **46**(2), 279–292.

Cossalter V, Lot R and Maggio F 2004 The modal analysis of a motorcycle in straight running and on a curve. *Meccanica* **39**(1), 1–16.

Cossalter V, Lot R and Massaro M 2007b The influence of frame compliance and rider mobility on the scooter stability. *Vehicle System Dynamics* **45**(4), 313–326.

Cossalter V, Lot R and Massaro M 2008 The chatter of racing motorcycles. *Vehicle System Dynamics* **46**(4), 339–353.

Cossalter V, Lot R and Massaro M 2011b An advanced multibody code for handling and stability analysis of motorcycles. *Meccanica* **46**(5), 943–958.

Cossalter V, Lot R and Massaro M 2012 The significance of powertrain characteristics on the chatter of racing motorcycles.

Cossalter V, Lot R, Massaro M and Peretto M 2010 Motorcycle steering torque decomposition, vol. 2, pp. 1257–1262.

Cossalter V, Lot R, Massaro M and Sartori R 2011c Development and validation of an advanced motorcycle riding simulator. *Proceedings of the Institution of Mechanical Engineers, Part D: Journal of Automobile Engineering* **225**(6), 705–720.

De Vries E and Pacejka H 1998 Motorcycle tyre measurements and models. *Vehicle System Dynamics* **29** (Suppl.), 280–298.

Katayama K, Aoki A, Nishimi T and Okayama T 1987 Measurement of structural properties of riders. *SAE paper 871229*.

Kiencke U and Nielsen L 2001 *Automotive Control Systems*. Springer-Verlag.

Lot R 2004 A motorcycle tire model for dynamic simulations: Theoretical and experimental aspects. *Meccanica* **39**(3), 207–220.

Lot R and Massaro M 2007 The kick-back of motorcycles: Experimental and numerical analsysis *Multibody Dynamics 2007, Eccomas Thematic Conference*.

Massaro M 2011 A nonlinear virtual rider for motorcycles. *Vehicle System Dynamics* **49**(9), 1477–1496.

Massaro M and Cole DJ 2012 Neuromuscular-steering dynamics: motorcycle riders vs car drivers.

Massaro M and Lot R 2010 A virtual rider for two-wheeled vehicles, pp. 5586–5591.

Massaro M, Lot R and Cossalter V 2011a On engine-to-slip modelling for motorcycle traction control design. *Proceedings of the Institution of Mechanical Engineers, Part D: Journal of Automobile Engineering* **225**(1), 15–27.

Massaro M, Lot, R. Cossalter V, Brendelson J and Sadaukas J 2012 Numerical and experimental investigation on the significance of rider on motorcycle weave. *Vehicle System Dynamics* **50**(S1), 215–227.

Massaro M, Sartori R and Lot R 2011b Numerical investigation of engine-to-slip dynamics for motorcycle traction control applications. *Vehicle System Dynamics* **49**(3), 419–432.

Nishimi T, Aoki A and Katayama K 1985 Analysis of straight running stability of motorcycles. *SAE paper 856124*.

Pacejka HB 2006 *Tyre and Vehicle Dynamics* 2nd edn. Butterworth-Heinemann, Oxford.

Sharp R and Limebeer D 2004 On steering wobble oscillations of motorcycles. *Proceedings of the Institution of Mechanical Engineers, Part C: Journal of Mechanical Engineering Science* **218**(12), 1449–1456.